Bioorganic Chemistry 86 (2019) 322–338

Contents lists available at ScienceDirect

Bioorganic Chemistry

journal homepage: www.elsevier.com/locate/bioorg

Toward a treatment of diabesity: Rational design, synthesis and biological evaluation of benzene-sulfonamide derivatives as a new class of PTP-1B inhibitors

Nagat Ghareb[a,b], Norhan M. El-Sayed[c], Reda Abdelhameed[f], Koji Yamada[d], Mohamed Saleh Elgawish[e,*]

[a] Pharmaceutical Organic Chemistry Department, Faculty of Pharmacy, Suez Canal University, Ismailia 41522, Egypt
[b] Chemistry Department, College of Sciences, Prince Sattam bin Abdul-Aziz University, Saudi Arabia
[c] Pharmacology and Toxicology Department, Faculty of Pharmacy, Suez Canal University, Ismailia 41522, Egypt
[d] Graduate School of Biomedical Sciences, Nagasaki University, 1-14 Bunkyo-machi, Nagasaki 852-8521, Japan
[e] Medicinal Chemistry Department, Faculty of Pharmacy, Suez Canal University, Ismailia 41522, Egypt
[f] Graduate school of biomedical sciences, Nagasaki University to Pharmacognosy Department, Faculty of Pharmacy, Suez Canal University, Ismailia 41522, Egypt

ARTICLE INFO

Keywords:
PTP1B inhibitors
Benzene-sulfonamide
Synthesis and biological evaluation
Molecular modeling, DFT calculation
In silico ADME prediction

ABSTRACT

Targeting of protein tyrosine phosphatase-1B (PTP1B) has emerged as a promising strategy for therapeutic intervention of diabetes and obesity. Investigation of new inhibitors with good bioavailability and high selectivity is the major challenge of drug discovery program targeting PTP1B. Therefore, herein, new neutral benzene-sulfonamide containing compounds were designed, synthesized and biologically evaluated as potent PTP1B inhibitors. New series of thiazolidine, oxazolidine, thiazinan, oxazinan, oxazole, thiazole, tetrazole, cyanopyridine, chromenone, and iminochromene of benzene-sulfonamide derivatives (**MSE-1 to MSE-15**) were synthesized in a good yield under mild condition using sulfadiazine as a starting material. Among the synthesized compounds, **MSE-13** and **MSE-14** showed the most *in vitro* potent PTP-1B inhibitory activity (IC_{50} of 0.88 μM and 3.33 μM, respectively). Animal treatment by the target compounds significantly improved the insulin resistance, diminished plasma glucose level, decreased initial body weight, and normalized the serum lipid profile compared to pioglitazone, a standard PTP1B inhibitor. The molecular modeling study showed a high affinity and selectivity of our synthesized compounds to the active site and B-site of PTP1B holding hydrogen bonding, hydrophobic, and electrostatic interactions. Furthermore, Electrostatic Surface Potential (ESP) and HOMO/LUMO analysis indicated the importance of sulfamoyl moiety for PTP1B binding. *In silico* ADME predictions of such compounds also showed the promising pharmacokinetic and physicochemical properties. The proposed compounds could be considered a lead inhibitory scaffold to PTP1B.

1. Introduction

Diabetes and obesity are major public health threats affecting more than one billion people globally [1]. International Diabetes Federation shows that the prevalence of type 2 diabetes in many Middle Eastern and North African countries are 1.5–2.5-fold that of the globe [2]. Anti-diabetic drugs, alongside a healthy diet and exercise routine, help a diabetic patient to maintain stable blood glucose levels. The current treatments including, sulfonylureas, thiazolidinediones, insulin secretagogues, have severe side effects such as hypoglycemia, weight gain, a risk of liver disease and other complications [3]. Therefore, there is a pressing need to develop more efficacious antidiabetic drugs. Therapeutic tactics targeting protein tyrosine phosphatase (PTP)-1B have emerged as a novel solution to the cure of diabetes, obesity, and cancer with minimum side effects [4]. PTP1B plays a vital role in regulating body weight, glucose homeostasis, and energy expenditure by acting as a key negative regulator of insulin and leptin receptor-mediated signaling pathways [5,6] PTP1B knockout mice are healthy with lowing plasma glucose and triglyceride levels through improving insulin sensitivity, glycemic control, and resistance against weight gain when placed on a high-fat diet (HFD) [7]. Consequently, the discovery of PTP1B inhibitors seems a promising strategy for therapeutic intervention of diabesity.

The crystal structure of PTP1B in complex with a p-Tyr substrate has been reported and found to be composed of a single catalytic domain

* Corresponding author.
E-mail address: mohamed_elgawish@pharm.suez.edu.eg (M.S. Elgawish).

https://doi.org/10.1016/j.bioorg.2019.01.052
Received 3 September 2018; Received in revised form 16 January 2019; Accepted 25 January 2019
Available online 31 January 2019

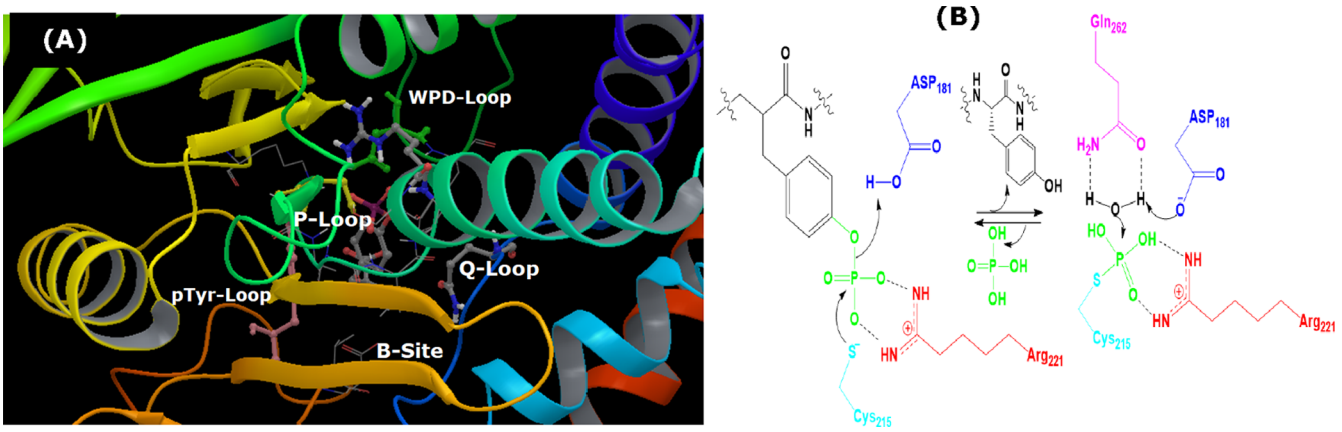

Fig. 1. (A) X-ray crystallographic structure of PTP1B catalytic domain and (B), PTP1B catalytic mechanism.

(residues 30–278) and various functional loops to regulate the dephosphorylation activity of proteins (Fig. 1A). The signature motif lies between residues 214 and 221, and Cys215 is the key nucleophilic residue responsible for its catalytic activity. Besides the P-loop, there are other binding sites including, the substrate recognition loop, P-Tyr loop, (Tyr46, Val49 and Lys120), Q-loop (Gln262), the WPD loop (Thr177 to Pro185), and the secondary binding site, B-site, (TYR20, ARG24, HIS25, ALA27, PHE52, ARG254, MMET258, GLY259). CYS215, ARG221, ASP181, and GLN262 are the key residues for the catalysis (Fig. 1B) [8,9]. Nevertheless, other residues which form hydrogen bonding, hydrophobic, and electrostatic interactions with the substrates are also significant. P-loop is conserved in all PTPs for binding the phosphate group and, consequently, the inhibitors binding solely to active site lack the desired selectivity. Despite the high homology model in the catalytic domain, *T*-cell (TC)-PTP and PTP1B regulate diverse biological functions. TCPTP knockout mice died within 3–5 weeks after birth owing to the defect in hematopoiesis and immune function [10]. Thus, it is an urgent need to discover new PTP1B inhibitors acting at alternative binding sites.

In the last two decades, various PTP1B inhibitors have been developed (Fig. 2), however, there is no drug approved as PTP1B inhibitor until now, and only two small drug-like molecules, Ertiprotafib and Trodusquemine, are entered clinical trial, but unfortunately these two drugs failed to get FDA approval due to the poor clinical efficacy, undesirable side effects, and limited financial resources, respectively [11] The efforts in developing PTP1B inhibitors have moved from early nonhydrolyzable phosphonic acid to various structures with diverse chemical entities. Nearly all upcoming drug development efforts have been discontinued because potent phosphotyrosine mimetic bioisosteres such as difluoromethyl phosphonate (DFMP), carboxylic or dicarboxylic acid, and heterocyclic thiazolidinone (TZD) and isothiazolinone (IZD) are negatively charged molecules with weak selectivity (especially TC-PTP), poor cell permeability, and low oral bioavailability, which shorten their applicability as novel therapeutic drugs [4,12,13]. Neutral or less acidic molecules thus introduce an alternative strategy for developing PTP1B inhibitors with favorable permeability and bioavailability.

B-site is a secondary binding site adjacent to the PTP1B active site. It is lined by non-conservative and electronically neutral residue and, consequently, targeting this site might be a practical strategy to achieve the desired selectivity and biological activity. B-site represents a remarkable structural part and can be exploited to the rationale design of potent and selective dual acting PTP1B inhibitors fitting both active and nearby sites [14]. Sulfamic acid moiety has been identified during a high throughput screening campaign as a potential p-Tyr mimetic in addition to phosphonic and carboxylic acids [15,16]. Incorporating sulfamic acid moiety into a tetrahydroisoquinoline scaffolds has shown a promising PTP1B inhibitory activity [15]. Extra-addition of the sulfamic acid moiety improves the biological activity multiple folds since two sulfamic acid moieties tightly bind both active site and B-site of PTP1B. The incorporation of sulfamic acid moiety to certain scaffold might achieve the coveted potency, however, the selectivity and poor permeability still remain the main obstacles facing the designing of these compounds. In an effort to discover potent and selective PTP1B inhibitors, dual binding of both P-loop and B-site would significantly promote the potency and selectivity owing to additive effects [14].

1.1. Rational and design

In this study, we imagine that neutral hydrogen bond acceptor moieties instead of negatively charged sulfamic acid group for hydrogen bonding in B-site could improve the cellular permeability, oral bioavailability, and selectivity. Our rationale concept is based on a chemical intuition that sulfonamide group, probably forms multiple hydrogen bonding interactions within B-site like sulfamic acid does. Neutral pyrimidine-sulfonamide containing compounds can achieve more selectivity over TCPTP. The Pyrimidine group could pick up hydrophobic interaction with amino acid residues in a wide and flat B-site of PTP1B. Improving the interactions of proposed compound with ASP48 and GLN262 in Q-loop may represent a good strategy for enhancing potency and selectivity [17]. Molecular modeling program postulated that ideal dual binding PTP1B should have aromatic and/or heteroaromatic, hydrogen bond donor and acceptor, and flexible linker. Hence the competitive inhibitors have to carry negative charge to compete with p-Tyr, but this negative charge has a poor impact on cellular permeability. We countered this problem by incorporating hydrogen bond acceptors in lieu of negatively charged p-Tyr isostere, such as thiazolidinone, tetrahydrothiazinone, oxazolidinone, tetrahydrooxazinone, tetrazole, chromenone, and iminochromene (Fig. 3). The designed compounds have been synthesized and their antidiabetic and anti-obesity have been evaluated compared to pioglitazone, a well-known PTP1B inhibitor. Furthermore, molecular modeling, Electrostatic Surface Potential (ESP) and HOMO/LUMO analysis, and *in silico* ADME prediction study have been established to confirm the success of our rational.

2. Results and discussion

2.1. Chemistry

Condensation of sulfadiazine, 4-amino-N-(pyrimidine-2-yl) benzenesulfonamide, with the appropriate isothiocyanate or phenyl isocyanate in DMF afford thioureido or ureido derivatives. The IR spectra of these compounds showed thiourea carbonyl band at 1090–1095 C m^{-1} and urea carbonyl at 1700–1708 C m^{-1} as well as

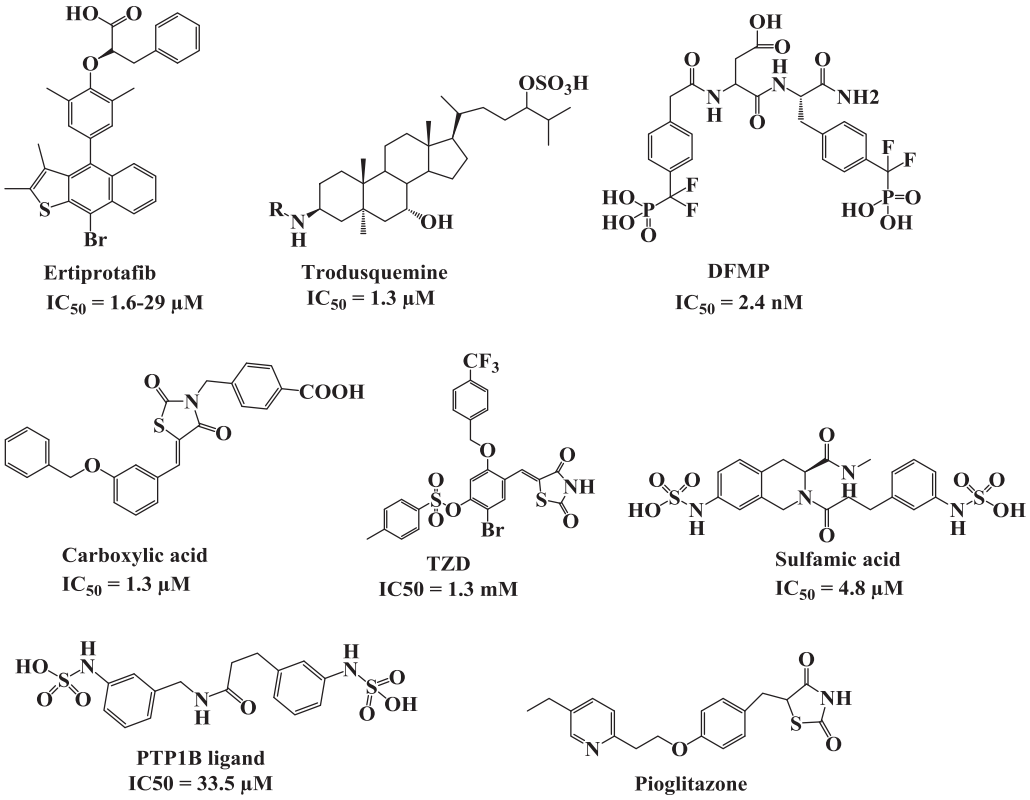

Fig. 2. Chemical structure and potency of some reported PTP1B inhibitors.

three bands at 3200–3209 C m^{-1}, 3350–3357 C m^{-1}, and 3420–3428 C m^{-1} due to NH groups. The ^{1}H NMR spectra of these compounds exhibited three singlet proton of NH groups at 9.92, 8.60, 8.59 ppm and aromatic protons at 6.14–7.74 ppm. Condensation of N,N-disubstituted urea or thiourea with chloroacetic acid gave 2-imino-5-oxo-thiazolidines/oxazolidines (**MSE-1** to **MSE-3**). This reaction proceeded through the intermediate formation of the cyclic pseudothiohydantoic acid [18]. The IR spectra of these compounds exhibited imino band (C═N) at 1635 C m^{-1}, cyclic carbonyl (C═O) group 1720 C m^{-1} as well as one NH group at 3379 C m^{-1}. The ^{1}H NMR spectra of these compounds exhibited a single signal of CH_2 of thiazolidine and oxazolidine rings at 4.27 ppm and disappeared of two singlet signal of two NH group of urea and thiourea. Ethyl group of **MSE-2** exhibited a triplet signal of CH_3 at 1.25 ppm and quadrat signal of CH_2 at 3.54 ppm. The ^{13}C NMR spectra of **MSE-2**, an example of these compounds, exhibited signal at 14.55 and 39.70 ppm corresponding to ethyl group attached to (N) of thiazolidine ring and a signal at 61.4 ppm of CH_2 of thiazolidine ring. Our thiourea derivatives were

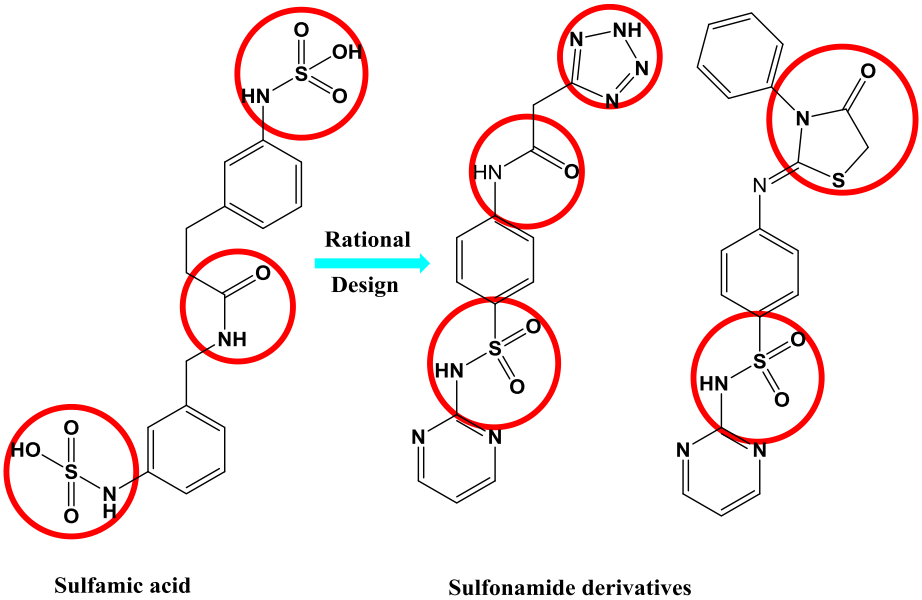

Fig. 3. Schamtic diagram of rational design of benzen-sulphonamide.

refluxed with ethyl-2-bromoropropionate or ethyl-3-bromoropropionate afforded 4-oxo-3-phenyl/methylthiazolidin-2-ylidene) amino, 5-methyl4-oxo-3-phenyl/methyl-thiazolidin-2-ylidene)amino, and 4-oxo-3-phenyl-1,3-thiazinan-2-ylidene)amino derivatives, respectively, whereas urea derivatives afforded 4-oxo-3-phenyloxazolidin-2-ylidene)amino and 5-methyl4-oxo-3-phenyl/methyl-thiazolidin-2-ylidene)amino (**MSE-4** to **MSE-6**). The IR spectra of these compounds exhibited imino band (C═N) at 1539 C m^{-1}, cyclic carbonyl (C═O) group 1724 C m^{-1} as well as one NH group at 3356 C m^{-1}. The ^{1}H NMR spectra of these compounds exhibited singlet signal of CH_2 of thiazolidine and oxazolidine rings at 4.28 ppm and disappeared of two singlet signal of two NH group of urea and thiourea owing to their incorporation into thiazolidine and oxazoldine rings. On another hand, condensation of thiourea and urea derivatives with phenacyl bromide in ethanol afforded 3,4-diphenylthiazol-2(3H)-ylidene)amino, 3,4-diphenyloxazol-2(3H)-ylidene)amino, 3-methyl, 4-diphenylthiazol-2(3H)-ylidene)amino derivatives (**MSE-7** to **MSE-9**). The IR spectra of these compounds exhibited imino band (C═N) at 1570–1575 C m^{-1} and one NH group at 3367 C m^{-1}. The ^{1}H NMR spectra of these compounds exhibited a singlet signal of CH of thiazole and oxazole rings at 6.14 ppm. While condensation of thiourea and urea derivatives with chloroacetyl chloride afforded 5-oxo-3-phenylthiazolidin-2-ylidene) amino, 5-oxo-3-ethylthiazolidin-2-ylidene)amino, and 5-oxo-3-phenyloxazolidin-2-ylidene)amino derivatives [18]. The IR spectra of these compounds exhibited cyclic carbonyl (C═O) at 1720 C m^{-1}, imino (C═N) at 1635 C m^{-1}, and amino (NH) at 3379 C m^{-1}. The ^{1}H NMR spectra of these compounds exhibited a single signal of CH_2 of oxazolidin and thiazolidin at 4.32 ppm. The ^{13}C NMR spectra of these compounds confirmed the cyclization and formation of thiazoldinone and oxazolidinone where *C*2 of these two rings and *C*2 of pyrimidine ring exhibited signal at 154.12 and 159.4 ppm, respectively. **MSE-10** was obtained by refluxing sulfadiazine with and carbonyldiimidazole in dry THF for 16 h [19]. The IR spectra of this compound exhibited urea carbonyl at 1700–1708 C m^{-1} as well as four bands from 3200–3400 C m^{-1} due to NH groups. Cyanoacetanilide, **MSE-11**, was synthesized by refluxing of sulfadiazine with ethyl cyanoacetate in dry DMF [20]. The reactivity of cyanoacetanilide towards sodium azide and ammonium chloride in DMF was investigated and found to give tetrazole derivative [21], **MSE-12**. The IR spectra of **MSE-12** exhibited carbonyl band at 1651 C m^{-1}, (C═N) bands range from 1408 to 1581 C m^{-1}. The ^{1}H NMR spectra of this compound exhibited singlet signal of CH_2 lie between tetrazole and carbonyl group at 3.55 ppm and The ^{13}C NMR spectra of the same compound exhibited signal at 39.70 ppm for the same CH_2. Cyclocondensation of **MSE-11** with acetylacetone in piperidine afforded pyridinone derivatives, **MSE-13**, in moderate yield. The IR of **MSE-13** showed a carbonyl (C═O) band at 1651 C m^{-1} and nitrile (C≡N) band at 2198 C m^{-1}. The ^{1}H NMR spectra of **MSE-13** exhibited two singlet signals of two CH_3 attached to pyridinone ring at 2.04 and 2.62 ppm. The ^{13}C NMR spectra of this compound also showed two signal at 22.53 and 22.15 ppm corresponding to two methyl group on pyridinone nucleus. Cyclocondensation of **MSE-11** with salicylaldehyde in ethanolic ammonium acetate afforded 2-iminochromene **MSE-14** in reasonable yield. The IR of **MSE-14** exhibited a carbonyl 1693(C═O) and three bands at 3155, 3452, and 3556 C m^{-1} owing to NH. The ^{1}H NMR spectra of **MSE-14** exhibited a single signle at 9.47 ppm of NH of iminochromene ring. The ^{13}C NMR spectra of **MSE-14** exhibited a signal at 39.62 ppm corresponding to aliphatic CH_2 of 2-iminochromene and two signal at 160.59 and 161.04 ppm corresponding to imino and carbonyl carbon. Whereas the reaction of cyanoacetanilide **MSE-11** with salicylaldehyde in the presence of AcOH/AcONa, a chromenone **MSE-15** was generated. The IR of **MSE-15** exhibited two carbonyl bands at 1666 and 1693 C m^{-1}. The ^{13}C NMR spectra of this compound also showed two signals at 160.61 and 161.07 ppm corresponding to two carbonyls carbon. The ^{1}H NMR and ^{13}C NMR spectra of designed compounds in **scheme-1** and **scheme-2** are available in the supplementary information.

2.2. Biological evalution

2.2.1. In vitro PTP1B inhibitory activity

The synthesized compounds were evaluated to test their *in vitro* ability to inhibit PTP-1B using Cyclex® Protein tyrosine phosphatase PTP1B Fluorometric Assay Kit. The assay was done according to the kit protocol (complete data incorporated in supplementary information). Pioglitazone served as a reference standard for comparison. Compounds **MSE-13** and **MSE-14** bearing cyanopyridinone and iminochromene backbones exhibited a potent PTP1B inhibitory activity with IC_{50} of 374.32 and 1260.04 ng/mL (0.88 and 3.33 μM, respectively). Under the same condition, pioglitazone exhibited a promising activity with IC_{50} of 242.63 ng/mL (0.68 μM). Additionally, the K_i values (the inhibition constant)of the most potent compounds (**MSE-13** and **MSE-14**) and the reference compound, pioglitazone, using the Cheng-Prussoff equation. It was found that K_i values are 0.39 μM, 1.48 μM, and 0.3 μM to MSE-13, MSE-14, and pioglitazone, respectively.

2.2.2. In vitro quantitative measurement of PTP1B in rat liver homogenate

The synthesized compounds were evaluated to test their *in vitro* ability to bind and/or denaturate PTP-1B after incubation with rat liver homogenate using PTP1B ELISA kit. The assay was done according to the kit protocol. Pioglitazone served as a reference standard for comparison. Compounds **MSE-13** and **MSE-14** bearing cyanopyridinone and iminochromene backbone exhibited potent PTP1B inhibitory activity with IC_{50} of 187.29 and 232.6 ng/mL (0.414 and 0.552 μM, respectively). Under the same condition, pioglitazone exhibited promising activity with IC_{50} of 147.92 ng/mL (0.414 μM).

2.2.3. Pharmacological study

In the current study, feeding rats with a high-fat diet (HFD) for 2 months produced a significant increase in body weight which was greater than that recorded in rats fed with a normal fat diet for the same period. Daily treatment with sulfonamide derivatives (2 mg/kg) reduced the body weight compared to HFD control group. All design compounds showed good results and both **MSE-13** and **MSE-14** effectively decreased body weight by 33%. Analysis of serum lipid profile demonstrated a significant increase in total cholesterol and triglycerides levels in rats fed with the HFD compared to normal rats. Repeated doses of our compounds (2 mg/kg) decreased total cholesterol and triglycerides with a higher efficacy (28%) shown by compounds **MSE-13 and MSE-14 (**Table 1**)**.

The present study also shows that the HFD group had significantly higher fasting plasma glucose and insulin levels with increased HOMA-IR compared to the normal group. Groups treated with sulfonamide derivatives showed promising antidiabetic activity especially compounds **MSE-13** and **MSE-14** which showed significantly decreased in FBG, insulin, and HOMA-IR compared to the obese control group (Table 2). Insulin levels and HOMA-IR in rats treated with remaining compounds were significantly lower than the HFD group. However, they had a significant effect on the fasting blood glucose. The improvement on FBG was calculated to be around 34.9% and 33.7%, whereas a decline of 44.6 and 43.5% in serum insulin were obtained by repeated oral gavages of compound **MSE-13** and **MSE-14,** respectively. The improvement in FBG and serum insulin leads to improvement of insulin resistance as evidenced by the HOMA index (Table 2) which was calculated to be around 33.8–63.3% to the target compounds.

2.3. Molecular docking

Docking study revealed that interactions of our designed compounds and PTP1B were dominated by the hydrogen bonding, hydrophobic and electrostatic interactions. ARG24, ARG254 in B-site, GLN262 in Q-loop, ARG47 and ASP48 in P-Tyr loop, and ALA217 were the main residues involved in hydrogen bonding. While ALA27, SER28, ASP29, PHE52, CYS32, and MET258 of the B-site were the main

Table 1
Effect of daily treatment with Sulfonamide-Azoles derivatives on percent increase in body weight and serum lipid profile in the experimental groups.

Groups	Body weight (gm)	Total cholesterol (mg/dl)	Triglycerides (mg/dl)
Negative control	162.2 ± 5.6	86.6 ± 3.4	82.8 ± 4.6
HFD (obese control)	271.6 ± 4.6*	139.6 ± 5.4*	128.5 ± 1.9*
HFD + MSE-1	233.6 ± 3.1#	122.4 ± 3.8#	112.2 ± 4.2#
HFD + MSE-2	234.2 ± 4.5#	125.2 ± 4.1#	116.4 ± 5.6#
HFD + MSE-3	231.7 ± 3.6#	124.4 ± 5.8#	113.2 ± 3.1#
HFD + MSE-4	227.2 ± 4.8#	120.1 ± 2.2#	108.1 ± 4.2#
HFD + MSE-5	226.4 ± 3.7#	118.3 ± 4.3#	111.5 ± 2.5#
HFD + MSE-6	223.5 ± 4.1#	116.4 ± 3.8#	107.2 ± 4.7#
HFD + MSE-7	235.6 ± 3.4#	127.2 ± 2.4#	117.6 ± 3.2#
HFD + MSE-8	237.1 ± 2.7#	129.4 ± 2.5#	118.3 ± 5.4#
HFD + MSE-9	238.3 ± 4.1#	127.2 ± 3.1 #	120.2 ± 3.8#
HFD + MSE-10	223.6 ± 3.2#	112.4 ± 5.2#	104.5 ± 4.2#
HFD + MSE-11	221.4 ± 5.1#	120.4 ± 4.1#	106.2 ± 4.2#
HFD + MSE-12	228 ± 5.7#	120.6 ± 4.8	110.5 ± 3.9#
HFD + MSE-13	183.8 ± 6.7#	100.4 ± 3.1#	88.1 ± 3.5#
HFD + MSE-14	184.6 ± 6.1#	101 ± 2.7#	88.5 ± 2.1#
HFD + MSE-15	230.6 ± 5.8#	122.6 ± 4.8#	114.4 ± 3.2#
Pioglitazone	275 ± 3.1#	138.4 ± 4.3#	127.3 ± 3.8#

Data are expressed as mean ± SEM. Data are analyzed by one-way ANOVA followed by Bonferroni's post hoc test.
* Significant from group 1 (negative control).
# Significant from group 2 (HFD obese group). Values of $p \leq 0.05$ were considered significant.

Table 2
Effect of daily treatment with Sulfonamide-Azoles derivatives on fasting blood glucose, fasting insulin, and HOMA-IR in the experimental groups.

Groups	Blood glucose (mg/dl)	Insulin (μU/ml)	HOMA-IR index
Negative control	83.8 ± 6.4	6.2 ± 0.2	1.40 ± 0.2
HFD (obese control)	163 ± 3.3*	17.7 ± 0.4*	7.10 ± 0.2*
HFD + MSE-1	138.6 ± 5.2#	11.9 ± 0.3#	4.10 ± 0.2#
HFD + MSE-2	135.6 ± 4.1#	12.1 ± 0.4#	4.05 ± 0.1#
HFD + MSE-3	133.8 ± 3.8#	12.6 ± 0.6#	4.1 ± 0.3#
HFD + MSE-4	122.3 ± 5.6#	11.2 ± 0.4#	3.38 ± 0.4#
HFD + MSE-5	124.6 ± 3.2#	10.6 ± 0.2#	3.26 ± 0.2#
HFD + MSE-6	121.3 ± 4.4#	10.3 ± 0.3#	3.08 ± 0.3#
HFD + MSE-7	140.7 ± 3.1#	12.3 ± 0.5#	4.27 ± 0.5#
HFD + MSE-8	144.1 ± 5.5#	12.7 ± 0.2#	4.5 ± 0.3#
HFD + MSE-9	146.6 ± 4.7#	12.5 ± 0.4#	4.52 ± 0.2#
HFD + MSE-10	119.5 ± 3.6#	10.7 ± 0.2#	3.15 ± 0.1#
HFD + MSE-11	117.2 ± 4.2#	10.4 ± 0.5#	3.01 ± 0.3#
HFD + MSE-12	132.2 ± 3.2#	12.8 ± 0.3#	4.2 ± 0.1#
HFD + MSE-13	106.7 ± 5.1#	9.8 ± 0.5#	2.6 ± 0.1#
HFD + MSE-14	108.2 ± 6.4#	10 ± 0.7#	2.7 ± 0.2#
HFD + MSE-15	140.6 ± 3.3#	13.8 ± 0.3#	4.7 ± 0.1#
Pioglitazone	100.2 ± 4.5#	8.8 ± 0.61#	2.17 ± 0.32#

Data are expressed as mean ± SEM. Data are analyzed by one-way ANOVA followed by Bonferroni's post hoc test.
* Significant from group 1 (negative control).
# Significant from group 2 (HFD obese group). Values of $p \leq 0.05$ were considered significant.

residues incorporated in hydrophobic interaction. The π-π interaction was established by TYR46 and PHE182 and aromatic and/or hetero-aromatic rings of designed compounds. ASP48, ARG24, and ARG254 are involved in a salt bridge and electrostatic interaction (Fig. 3, supplementary information). These interaction forces afforded the promising affinity and high selectivity to PTP1B. Extra precision glide docking of our proposed compounds showed good G or docking score and glide Emodel. The binding affinity representing by the previous scores were compared to reference compounds (Table 1, supplementary information). **MSE-14** showed high docking score (−5.40 KJ/mol) which simulates a binding free energy. Highest negative values of **MSE-14** represent tighter binders that attributed to three hydrogen bonding with ARG254 (2.03 Å), ARG24 (2.02 Å), and GLN262 (1.96 Å) (Fig. 4). The docking of PTP1B ligand containing sulfamic acid moiety shows higher docking score value (−9.02 KJ/mol) owing to nine hydrogen bonding in active, recognition substrate, Q-loop, and B-sites. Whereas pioglitazone showed lower docking score (−4.13 KJ/mol) than **MSE-14** resulting from one hydrogen bonding interaction with ARG254 (2.66 Å) (Fig. 4). The selectivity of the designed compounds towards PTP1B is proven by docking the most potent compounds within the active site of TCPTP, the phosphatase most closely related to PTP1B (Fig. 1. supplementary information). The designed compounds showed weak affinity towards TCPTP active site and B site (PDB ID 1L8K).

Moreover, the accuracy of the docking procedure was evaluated by determining how closely the lowest energy poses predicted by the docking score and/or Glide score almost match an experimental binding mode as determined by X-ray crystallography. The root means square deviation (RMSD) between the predicted conformation and the observed X-ray crystallographic conformation of sulfamic acid ligand (PDB ID: 2F70) equal to 1.002 Å (Fig. 2 supplementary information), a value that indicated the reliability of Glide XP docking. 2D of ligand-receptor interaction generated by our experimental resembled one detected by X-ray crystallography. The same pose and same type of ligand-protein interactions were found (Fig. 2. supplementary information).

2.4. Computational study

The energy calculation in Gaussian 09 software using Density Functional Theory (DFT) method on the crystallized conformation of sulfamic acid derivatives, lead molecule, and the docked conformation of compound **MSE-14** was run to visualize the charge distribution on both compounds, to better understand the chemical reactivity of molecules, and to estimate the contribution of polar and nonpolar interactions in their binding to PTP1B. The B3LYP functional was employed with 6-311 + +G (d, p) basis set to calculate the Mulliken charge distribution for all the atoms as well as the Electrostatic Surface Potential (ESP) for **MSE-14** and sulfamic acid derivative. In Fig. 5A, Mulliken atomic charges showed the negative charge of the aromatic center that indicated a high electron density causing π-π interaction. The calculated atomic charge of the sulfamic acid oxygen and sulfonamide oxygen of **MSE-14** interacting with ARG24 and ARG254 in site B was found to be (−0.513 to −0.678). This fortified the hydrogen bond (HBA) formation and highlighted the significance of interaction for PTP1B selectivity. Interestingly, the high negative atomic charge of sulfonamide NH expected salt bridge formation with ARG24 and ARG254 in site B or ionic bond formation with ASP48 in p-Tyr-loop. Moreover, the hydrogen bond formation with GLN262 was attributed to the atomic negative charge of carbamoyl NH (Fig. 5A). Shape and size resemblance is apparently observed in the ESP of both compounds (Fig. 5B) with mostly two arms. The noticeable difference is the strong positive charge localized on the left arm of sulfamic acid PTP1B ligand that gives it the superiority to tightly bind within B-site. This, to some extent, explained the inhibitory power of sulfamic acid containing derivatives towards PTP1B. Generally, the appearance of electronegative and electropositive regions illustrates the ability of theses region to act as electron donor or acceptor to PTP1B active site. Docking result came in agreement with that; sulfonamide and carbamoyl moiety of designed compounds are involved in important interaction with the key residue of B and substrate recognition sites.

The orbital energies of HOMO and LUMO of the most active compound, **MSE-14** and lead sulfamic acid compound were calculated using Gaussian 09 software. Mechanistically, in ligand-protein interaction, the electron acceptor capability of the LUMO showed a significant role than the electron donation of the HOMO. The HOMO and LUMO sites were plotted on the molecular surface of two compounds as shown in

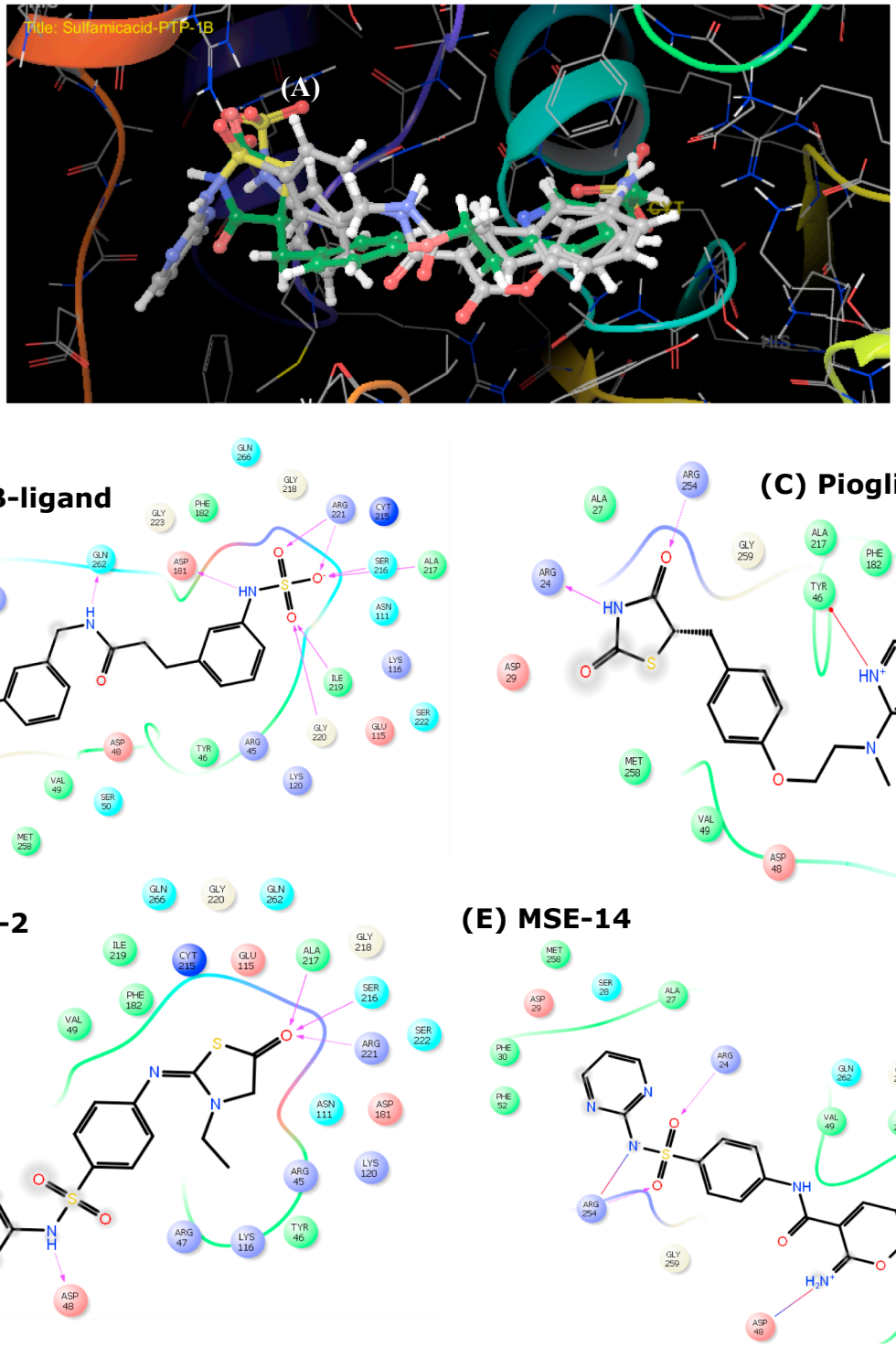

Fig. 4. (A) 3D-Binding mode of PTP1B-ligand, pioglitazone, and MSE-14 in the catalytic domain of 2F70. 2D-ligand interaction diagram of PTP1B ligand (B), Pioglitazone (C), MSE-2 (D), MSE-14 (E).

Fig. 6. Analysis of HOMO maps of compounds showed that HOMO molecular orbitals are located on sulfonamide and sulfamic acid moieties, indicating their involvement in protein-ligand interaction. On another hand, the LUMO molecular orbitals are located on sulfonamide and pyrimidine moieties of **MSE-14** and on the second sulfamic acid moiety of PTP1B ligand. Docking study revealed the involvement of these moieties in hydrogen bond formation with key residues of active and B-sites. The LUMO molecular orbital localized on the second sulfamic acid moiety of PTP1B ligand (Fig. 6) indicated potent interaction within the active site by hydrogen bond binding. This interaction gives the PTP1B ligand superiority as a PTP1B inhibitor. However, this interaction also weakens the selectivity over TC-PTP and diminished pharmacokinetic properties. Whereas, **MSE-14** lacked the molecular orbital localization on an imino-chromene moiety, which occupied active site (Fig. 5). Although this phenomenon weakens the affinity to PTP1B, it is improved the selectivity and pharmacokinetic properties, which are the main goals of this study.

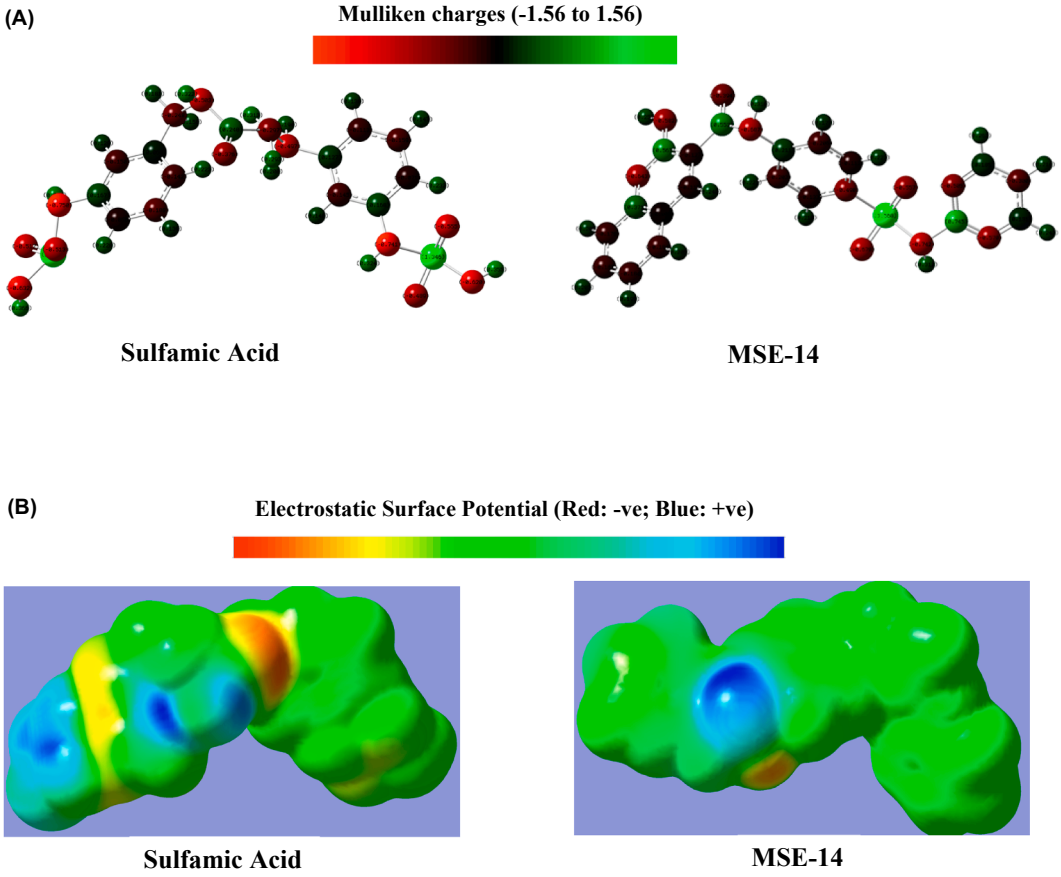

Fig. 5. (A) Mulliken charges, (B) Electrostatic Surface Potential (ESP) calculated using DFT method with B3LYP functional and 6-311 + +G (d, p) basic set methodology (color-coded from red to blue).

2.5. Lipinski's rule for drug likeliness and in silico ADME prediction

Various pharmacokinetic parameters of the target compounds were calculated utilizing ADME predictions by QikProp v4.3. The compounds were estimated for their fundamental parameters of Lipinski's rule of 5 and other pharmacokinetic parameters. Table 3 exhibited the results got from QikProp with their permissible values. A rule of thumb, an orally active compound should not have more than two violations of the Lipinski rule. The target compounds in this study were not violate the rule more than the maximum permissible limits and consequently proving their drug-likeness properties. The oral bioavailability of the drug molecules could be controlled by the value of rotatable bonds

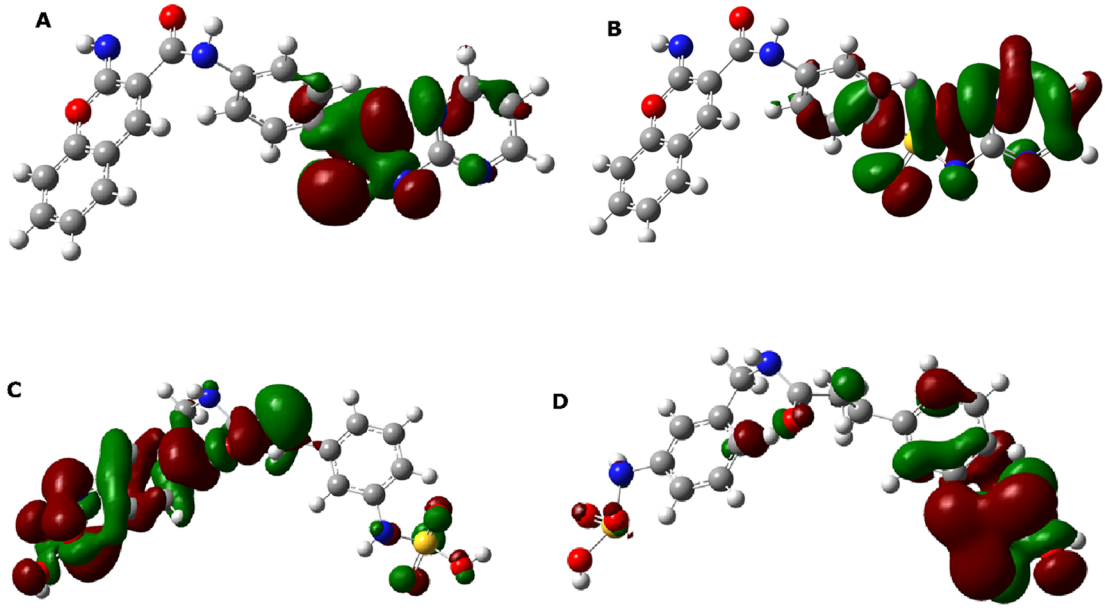

Fig. 6. Plots of HOMO and LUMO of MSE-14 (A, B) and sulfamic acid PTP1Bligand (C, D).

Table 3
In Silico ADME prediction parameters of designed and reference molecules.

Comp. No.	mol_MW[a]	donorHB[b]	accptHB[c]	QPlogPo/w[d]	#rotor[e]	PSA[f]	QPlogS[g]	QPlogHERG[h]	QPPCaco[i]	QPPMDCK[j]	QPlogKhsa[k]	% Human Oral Absorption [l]
MSE-1	425.47	1	9.5	2.039	5	116	−3.46	−5.51	268.99	225.61	−0.31	82.37
MSE-2	377.43	1	10	1.197	6	120	−3.31	−5.69	162.48	129.61	−0.61	73.52
MSE-3	409.42	1	9.5	2.45	5	126	−3.48	−5.57	279.56	231.22	−0.34	84.39
MSE-4	439.50	1	10.5	2.15	5	111	−3.45	−5.58	523.08	425.63	−0.37	88.19
MSE-5	391.46	1	10.5	1.50	6	111	−3.27	−5.49	328.57	262.34	−0.58	80.78
MSE-6	423.45	1	10.5	2.19	5	111	−3.51	−5.64	554.32	432.24	−0.39	90.12
MSE-7	485.57	1	7.5	4.68	5	83	−5.61	−6.70	1104.51	−0.55	0.55	100.00
MSE-8	469.51	1	8	4.04	5	93	−4.8	−6.64	1024.47	−0.68	0.36	100.00
MSE-9	421.47	1	8	3.38	6	97	−4.81	−6.89	577.95	−1.10	0.14	96.18
MSE-10	526.54	4	15	0.15	8	194	−4.70	−7.30	13.57	7.14	−0.95	22.18
MSE-11	317.32	2	10	−0.19	6	136.9	−3.64	−6.13	61.60	24.65	−0.89	57.82
MSE-12	360.35	3	12.5	−0.92	6	175	−2.83	−6.17	18.33	6.65	−0.97	31.17
MSE-13	381.40	1	11	0.78	4	128	−4.64	−6.21	98.23	40.84	−0.61	67.22
MSE-14	421.43	2	9.5	2.08	6	138	−4.77	−7.45	114.80	48.33	−0.16	76.01
MSE-15	422.41	1	10.5	1.58	5	146	−4.31	−7.34	95.71	39.70	−0.40	71.67
Pioglitazone	356.43	1	4.75	3.91	7	93.51	−5.56	−5.90	477.22	334.21	0.49	100.00
PTP1B-ligand	429.46	5	11	0.13	11	191	−2.8	−1.6	0.137	0.1	−1.34	12.25

Acceptable ranges:
[a] < 500 amu.
[b] < 5.
[c] < 10.
[d] < 5.
[e] 0–15.
[f] 7–200.
[g] < 0.5.
[h] < −5.
[i] < 25 poor, > 500 great.
[j] < 25 poor, > 500 great.
[k] −1.5–1.5.
[l] > 80% is high, < 25% is poor.

(0–15) and polar surface area (7–200 Å). Intestinal absorption or permeation is also one of the important factors for drug absorption study which was further confirmed by predicted Caco-2 cell permeability (QPPCaco), used as a model for the gut-blood barrier by non-active transport. Caco-2 cell permeability of the test compounds showed good results predicting excellent drug permeability. The cell permeability of the blood brain barrier was expected by QPPMDCK descriptor. MDCK cells are a good mimic for the blood-brain barrier. Most test compounds exhibited good BBB permeability (QPPMDCK > 25). Another important descriptor is QPlogkhsa descriptor of QikProp that predict human serum albumin binding capability. Our compounds showed reasonable binding to plasma proteins. QPlogPo/w and QPlogS are descriptors of the octanol/water partition coefficient and aqueous solubility; the test compounds were found to be in the permissible range (Table 3). The proposed compounds were considered promising lead molecules for designing potent PTP1B inhibitors with excellent membrane permeability and oral bioavailability. Physicochemical properties of the designed compound were enough to permeate our drug through GIT. **MSE-7** and **MSE-8**, have two phenyl rings substituted thiazolidine and oxazolidine ring, showed the highest partition coefficient and consequently highest penetration disclosed by the great value of QPPCaco and human oral absorption %. Moreover, *in silico* ADME prediction results came in agreement with *in vivo* study; **MSE-14** achieved the superior antidiabetic and anti-obesity activity that attributed to its reasonable oral bioavailability and membrane permeability and high affinity to PTP1B expected by *in silico* ADME and molecular modeling study. Alternatively, pioglitazone showed excellent *in silico* ADME result including, good partition coefficient, permeability and oral bioavailability (Table 3). Whereas PTP1B ligand, sulfamic acid derivative, showed the highest docking score and highest inhibitory activity, however, the *in silico* ADME results were very poor. Two sulfamic acid moieties improved its selectivity and affinity and diminished its partition coefficient, its permeability, and its oral absorption (12.5%).

Development of new antagonist with good bioavailability and cellular permeability is a major challenge in drug discovery program targeting PTP1B [4,22]. The negatively charged of PTP directed active site-pharmacophores to pTyr mimetics causes a poor membrane permeability and limits the further progress of such compounds as drug candidates [12]. In this regard, the trials in developing PTP1B inhibitors have changed from early nonhydrolyzable phosphonic acid derivatives to diverse molecules with various chemical and physical properties. Bioisosteric of p-Tyr with DFMP, carboxylic or dicarboxylic acid, and heterocyclic TZD or IZD have been developed achieving promising anti-obesity and antidiabetic activities (Fig. 2), however, most of these scaffolds are still negatively charged with poor bioavailability and cellular permeability to drive robust *in vivo* efficacy [11]. Charge reduction or even neutral molecules thus are an alternative approach in developing less potent PTP1B inhibitors with improved bioavailability and physicochemical properties [14]. The selectivity owing to the conserved active site, P-loop, is another challenge hinders the medicinal chemist for designing specific PTP1B inhibitors. The crystal structure of PTP1B shows four binding sites (Fig. 1): recognition loop, Q-loop, WPD-loop, and B-site, besides the catalytic site [8,9]. These secondary noncatalytic binding sites adjacent to the PTP1B active site are poorly conserved and, consequently, targeting these sites can overcome the selectivity issue. Zhang *et al* have succeeded to design dual binding inhibitors that occupy both the catalytic site and the B-site [23]. The designed molecules have shown antidiabetic activity and high selectivity. Many compounds after Zhang study have been developed and unambiguously confirmed that binding in the B-site provides not only more potent inhibitors but improved selectivity over the highly homologous phosphatase, TC-PTP [17].

Nevertheless, in an effort to overcome the major pharmacokinetic and selectivity problems, structure-based design, as well as virtual screenings and fragment-based approaches, have been applied to

discover lead PTP1B inhibitor with drug-like properties [24].The recent patent by P& G discloses that the inclusion of arylsulfamic acid, p-Tyr mimetic, can generate a potent small molecule with high selectivity towards PTP1B. In this study, we selected sulfamic acid derivatives as a lead compound [4]. PTP1B (PDB ID 2F70) ligand that contains two sulfamic acid moieties (Fig. 2), was selected as the starting compound to establish structure-based design of our novel drug-like molecules. This compound shows high affinity to PTP1B where one of arylsulfamic acid moiety occupies B-site forming hydrogen bonds with ARG254 and ARG24, whereas the second sulfamic acid moiety forms hydrogen bonds with SER216, ALA217, GLY220, and ARG221 in the catalytic site [15]. Additionally, the amino group of acetamide linker also forms a hydrogen bond with GLN262 in Q-loop (Fig. 4). Arylsulfamic acid ligand shows high potency (IC_{50} = 33.5 μM) with twofold selectivity over TCPTP and five-fold over other PTPs. We attributed the potency and high selectivity of the lead compound to occupancy of B-site forming two hydrogen bonds besides the hydrogen bonding with GLN262 in Q-loop. However, this lead compound suffers from poor cellular permeability and bioavailability (its human oral absorption is 12.25%) and, consequently, exhibits weak *in vivo* activity (Table 3). Considering the multiple challenges including bioavailability, specificity, and potency. Our rationale to design potent PTP1B inhibitors was based on keeping the hydrogen bonding interaction with key anchor points in B-site, ARG254, and ARG24. In designing of our compounds, the arylsulfamic acid moiety was replaced with the pyrimido-sulfonamide moiety (Fig. 3). The new moiety is neutral and lacks anionic charge of sulfamic acid and thus the bioavailability and specificity challenges are quenched (Table 3). Oxygen of sulfamoyl group can interact by hydrogen bonding with ARG24 and ARG254. Salt bridge between NH of sulfamoyl moiety and ARG24 and ARG254 was another interaction, which increased the affinity and drug-protein interaction stability. Mulliken charge distribution and ESP showed that sulfamoyl moiety is favorable for ligand-protein interaction. Pi-cation interaction of pyrimidine and ARG254 was also generated in some instance by our compounds (Fig. 3 supplementary information). Moreover, pyrimidine ring can interact with hydrophobic residues of B-site, PHE52, and MET258 (Fig. 4). Although the interaction with ARG254 and ARG24 is considered as the sole way to design specific PTP1B inhibitor, many of subsequent studies disclose that interaction with hydrophobic residues such as PHE52, MET258, and CYS32, could enhance antidiabetic activity and give the designed inhibitors the superiority against PTP1B [25]. On another hand, HIS34 and TYR54 are the corresponding amino acid residues in TCPTP which are bulky and more hydrophilic to interact like the residues in PTP1B (Fig. 1. Supplementary information). Pyrimidine ring is optimum for selectivity and could fully occupy the largely hydrophobic region of B-site, whereas phenyl ring could not provide the specificity over TCPTP [17]. The reason for pyrimidine specificity could be attributed to the interactions with surrounding amino acids (ASP29, VAL49, GLY259). The substrate recognition loop, composed of TYR46, VAL49 and LYS120, and ASP48, lays fairly near to catalytic site and targeting this site could nourish the design and synthesis of selective PTP1B inhibitors. In this study, we took into consideration the design of compounds that can interact with amino acid residues in this site. Aromatic ring attached to sulfamoyl moiety is interacted by hydrophobic or Van der Waal interaction with recognition loop amino acid, TYR46 and VAL49 (Fig. 4). The π-π interaction was also established by TYR46 and aromatic center of the designed compound. Xin *et al* have reported that interaction with LYS120 and TYR46 might improve the selectivity over TCPTP [26]. Moreover, ASP48 could also interact by the hydrogen bond or salt bridge with sulfamoyl moiety or the nitrogen of thiazole ring of the design compounds. The interaction with ASP48 at the edge of the catalytic site might improve molecular selectivity [17].

A poor cellular permeability of phosphonate group inspired the medicinal chemist to discover new functionality. DFMP, carboxylic or dicarboxylic acid, heteroaromatic rings, TZD and IZD (Fig. 1) are the bioisostere of the phosphonate group, which showed promising biological activity but still lack membrane permeability [4]. Therefore, in this study, we continued the development of a new ring system to improve bioavailability while keeping biological activity. The designed compounds should interact with the catalytic site in a manner similar to pTyr mimetics. Our rationale in this issue was to incorporate hydrogen bond acceptors in lieu of negatively charged p-Tyr isostere. Thiazolidinone, tetra-hydrothiazinone, oxazolidinone, tetrahydrooxazinone, tetrazole, chromenone, and iminochromene were selected as new scaffolds to overcome pharmacokinetic and physicochemical properties of the reported molecules. According to *in silico* ADME prediction, these scaffolds showed good bioavailability and membrane permeability (Table 3). In series A of our designed compounds in the **scheme-1** (**MSE-1** to **MSE-9**), It was found that the bulkiness around new scaffold could affect biological activity. Methylate-5-oxo-thiazolidine of **MSE-2**, for example, was occupied the only catalytic site and formed hydrogen bonding with the main amino acids residue of dephosphorylation, ALA217, SER 216, ARG221 (Fig. 4). Increasing the bulkiness on thiazolidine by one phenyl group such as **MSE-1** or two phenyl groups such as **MSE-7** hindered the reaching of thiazolidine or oxazolidine within the catalytic site (Fig. 3. supplementary information). These compounds kept the reaction with amino acid residue in site-B like all compounds. The compounds in **scheme-1** also reacted by hydrogen bonding or hydrophobic interactions with the substrate recognition site, ASP48, TYR46, VAL49. Lacking the reactivity to catalytic site or B-site moderated the binding affinity and antidiabetic and anti-obesity activity (Tables 1 and 2). Another important issue is the distance between aromatic center and the new scaffolds. The the aromatic center is linked to the new scaffolds via one atom, amino group (NH). The shortness of the linker hindered the occupancy of either catalytic site or B-site by the series A of **scheme-1** and can affect the pharmacological activity [27].

We envisioned that the linker length markedly affected the inhibitory activity against PTP1B. Increasing the length from two to three atoms improved binding affinity and *in vivo* biological activity. The compound of series B in Scheme-2 exhibited the highest affinity and antidiabetic activity. Two or three atoms linker allowed the design compounds to better fitting in both catalytic and B sites. Target compounds in scheme-2 (**MSE-10** to **MSE-15**) showed the same hydrophobic interaction, hydrogen bonding interaction, salt bridge, and pi-cation interaction with amino acids residue in site-B as compounds in Scheme 1 (Figs. 3 and 4, supplementary information). The novelty in Scheme 2 was linker composition and scaffolds occupied the catalytic site. On one hand, the incorporation of hydrogen bond acceptor or donation could improve the specificity and affinity. Urea or thiourea in our compounds showed hydrogen bonding interaction with the main amino acid of Q-loop, GLN262. The significance of the NH group in enhancing the PTP1B inhibitory activity, due to hydrogen bond formation, has been previously disclosed [28]. Despite, GLN262 isn't a residue of the catalytic site, it plays a vital role in restoring of CYS215 (Fig. 1). Therefore, the interaction with GLN262 residue might consider a favorable intervention to design a potent inhibitor (Fig. 4). The high negative atomic charge of NH in Mulliken charge distribution (Fig. 5) confirmed the willing of this group to hydrogen bond binding. On another hand, the rationale to improve cell permeability and oral bioavailability are to reduce the acidity of p-tyrmimetic. Thus, in this regard, new scaffolds including, tetrazole, chromenone, and iminochromene were designed to obtain inhibitor endowed with appropriate polarity and bioavailability. Tetrazole, a well known carboxylic bioisostere, was selected because carboxylic acid moiety has been reported as potent p-tyrmimetic. Tetrazole, diffusely anionic heterocycle, was deeply penetrated the catalytic site and form hydrogen bonding interaction with ALA217, pi-cation interaction and pi-pi stacking interaction with ARG221, PHE182, and hydrophobic interactions with CYS215, SER216, ILE219, GLY220, and LYS120 (Fig. 1, supplementary information). Tetrazole containing-compound, **MSE-12**, showed a promising binding affinity, membrane permeability, and

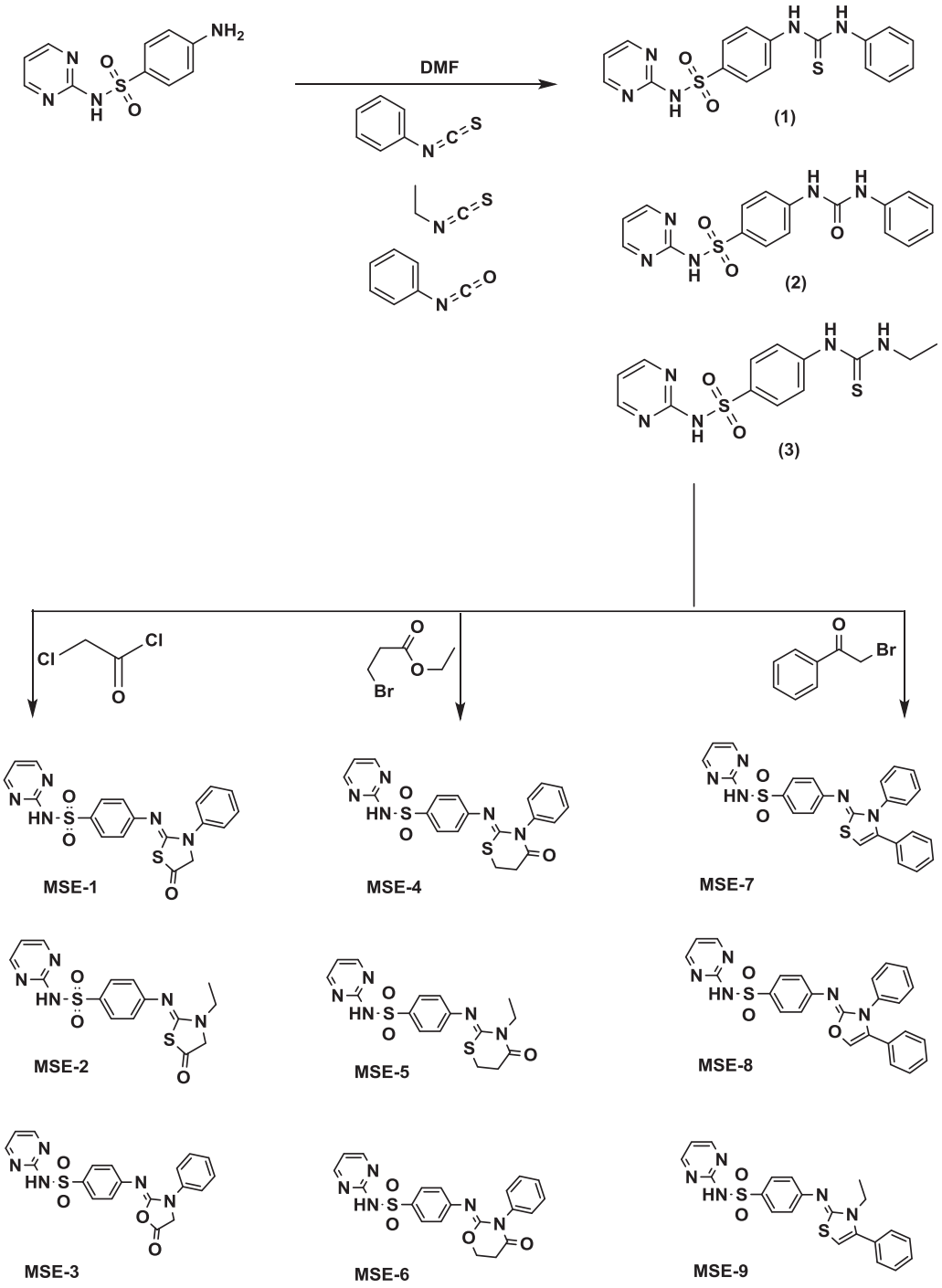

Scheme 1.

biological activity (Tables 1–3). **MSE-12** decreased body weight by 16% and FBG by 19%. The deep penetration of tetrazole ring to the catalytic domain of PTP1B prevented **MSE-12** to fully occupy B-site. **MSE-12** exhibited hydrogen bonding, π-π stacking interaction, and hydrophobic interaction with the substrate recognition loop, ASP48, TYR46, and ARG47 (Fig. 2, supplementary information).

Increasing ring size to bicyclic system prevented the deep penetration to catalytic domain allowing the designed compounds to occupy both the catalytic site and B-site achieving the main goal of this study. Chromenone and iminochromene, bicyclic systems, were selected as new scaffolds to overcome the bioavailability and selectivity. This bicyclic system is large enough to not deeply penetrate catalytic site and thus it could occupy also B-site achieving the desired activity. **MSE-14** and **MSE-15** were interacted with the catalytic site by hydrophobic interaction and with substrate recognition site by π-π stacking interaction, hydrophobic interaction and salt bridge formation between C═NH and ASP48. Additionally, these compounds interacted with the WPD loop by hydrophobic interaction, with Q-loop by hydrogen bonding, and with B-site by hydrogen bonding, salt bridge, and hydrophobic interactions (Fig. 4, Fig. 3, supplementary information). Thus **MSE-14** and **MSE-15** could interact with all catalytic domain of PTP1B by various type of interactions. Therefore, these compounds showed the highest binding affinity and the highest biological activity. These compounds represented a new trend in developing a PTP1B inhibitor, which showed poor interaction with the catalytic domain [4,8]. **MSE-14** showed a significant antidiabetic and antihyperlipidemic

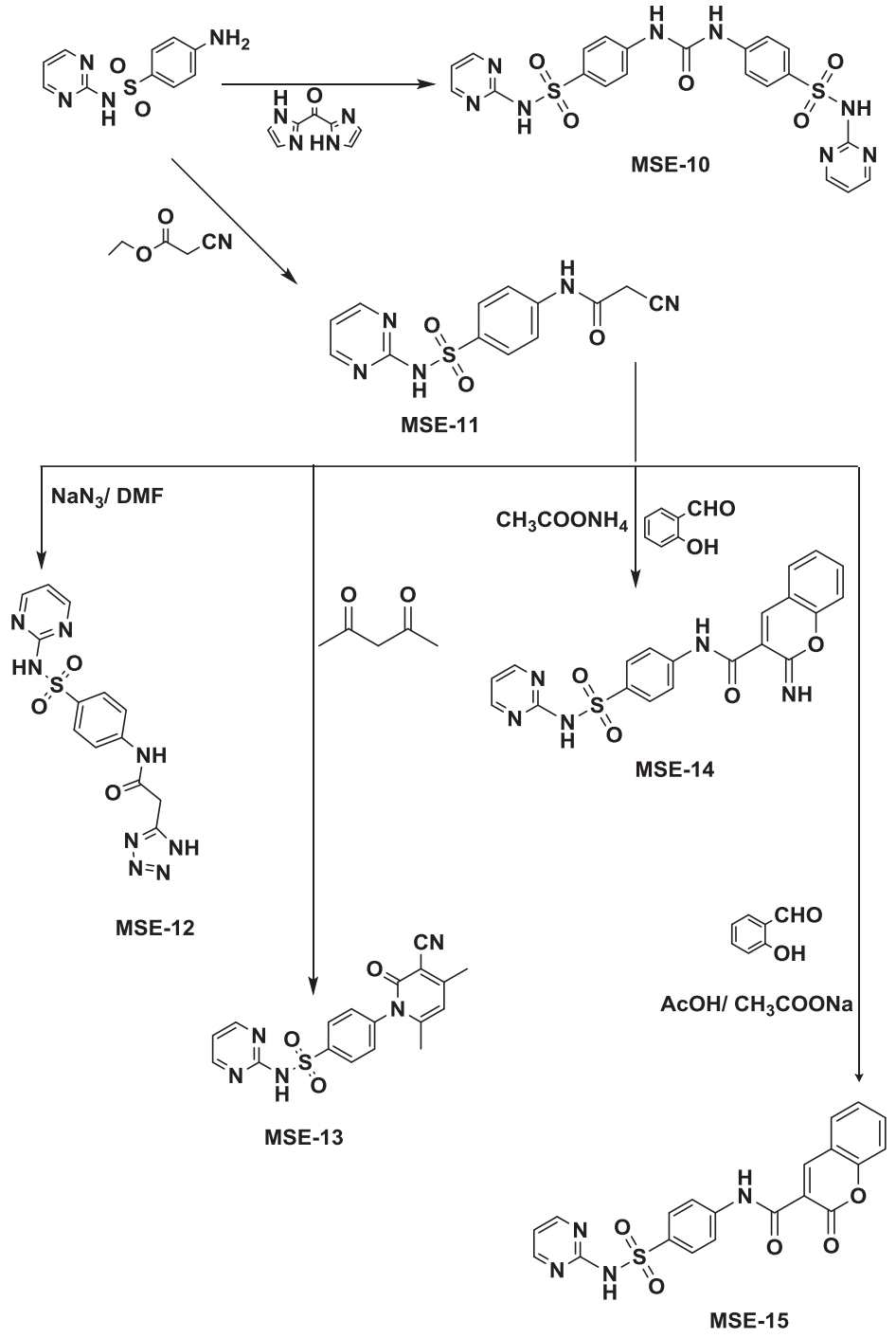

Scheme 2.

activity. **MSE-13** had the unique pose in PTP1B, where it occupied site-B and can't invade the catalytic site deeply. It interacted by hydrogen bonding with GLY259, ARG24, GLN262, and LYS36, salt bride with ARG254, and hydrophobic interaction with amino acid residues of site-B (Fig. 2, supplementary information). **MSE-13** was the only compound in this study which, deeply penetrate B-site; it could react with CYS32, the amino acid residue gave the selectivity towards PTP1B [25]. **MSE-13** showed a promising *in vitro* inhibitory potency (IC_{50} of 0.88 μM) and *in vivo* biological activity as shown in Table 1 and Table 2. Structure-activity relationship of designed compounds holding on catalytic domain of PTP1B summarized in Fig. 7.

Moreover, pan assay interference compounds (PAINS) was also utilized to confirm the biological activity of the designed compounds. Three standard filters, PAINS1, PAINS2, and PAINS3, of Canvas 2.3 function of Schrodinger 10.1 were used. All the designed compounds passed all the filters confirming their antidiabetic and anti-obesity activity. Rat body weight was decreased by 31.8%, cholesterol by 28%, while TG by 31%. We observed that **MSE-14** diminished weight gain by increasing metabolic rate not by decreasing food intake. Blood glucose was declined by 33.6% and serum insulin by 43.5% and thus there is an improvement in insulin resistance as shown by the HOMA index (Table 2). Insulin resistance is known to be the common link between obesity and diabetes.

To confirm the potency of our compounds as new scaffolds for

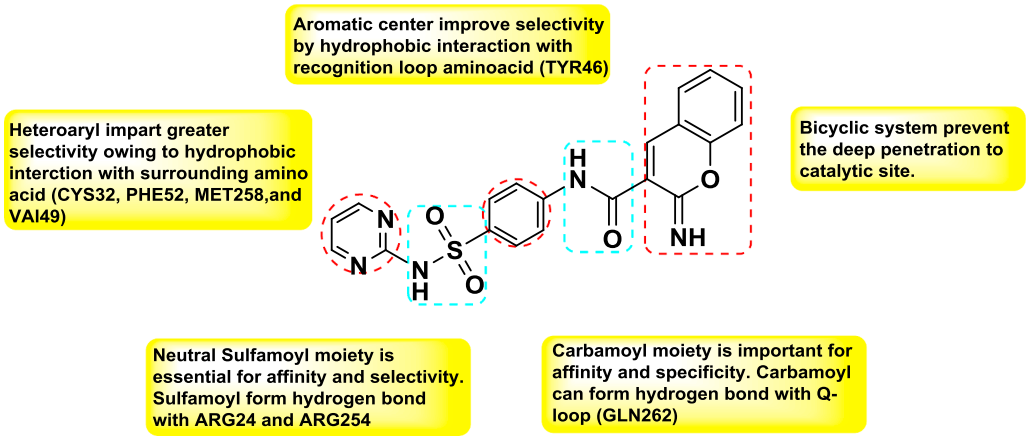

Fig. 7. Structure activity relationship of benzene-sulphonamide derivatives on catalytic domain of PTP1B.

deregulation PTP1B, pioglitazone was selected as a reference molecule. Pioglitazone, a PPARγ- agonist, is 2,4-thiazolidinedione (2,4-TZD) containing compound selected by other laboratories as PTP1B inhibitor [29,30]. *In vitro* inhibitory actvity of the most potent compounds against PTP1B using Fluorimetric assay kit disclosed that **MSE-13** and **MSE-14** were with promising activity (IC_{50} of 0.88 and 3.33 μM) compared to pioglitazone (IC_{50} of 0.68 μM). Using the Cheng-Prussoff equation. It was found that K_i values are 0.39 μM, 1.48 μM, and 0.3 μM to MSE-13, MSE-14, and pioglitazone, respectively. Comparing the values of IC_{50} and the inhibition constant (K_i), it was found that IC_{50} of the most active and reference is larger than the K_i value and thus our compound could competitively inhibit the PTP1B. Additionally, **MSE-13** and **MSE-14** were able to bind to PTP1B in liver homogenate of rat and specifically modify or denaturate PTP1B preventing the quantitative measurement using ELISA kit. **MSE-13** and **MSE-14** exhibited potent PTP1B inhibitory activity with IC_{50} of 187.29 and 232.6 ng/mL (0.414 and 0.552 μM, respectively). Under the same condition, pioglitazone exhibited promising activity with IC_{50} of 147.92 ng/mL (0.414 μM).

In biological screening, we found that pioglitazone does not significantly affect lipid profile, but positively affect body weight. Pioglitazone likes other antidiabetic drugs increases the body weight [3]. On another hand, pioglitazone has shown a marked effect on both FBG, serum insulin, and insulin resistance representing by HOMA-IR (Table 2). Pioglitazone can diminish insulin resistance in liver, muscle, and adipose tissue and improve lipid and glucose metabolism. FBG diminished by 38.6% and serum insulin by 50.2%. Furthermore, in a molecular modeling study, the designed compounds showed the same pose of PTP1B ligand and might interact with amino acid residue in the same manner (Fig. 4). However, pioglitazone has its unique pose, where thiazolidinedione moiety occupies B-site and interacts with ARG254 by hydrogen bonding. Whereas pyrimidine ring occupies the active site and interacts with amino acid residue by hydrophobic interaction. This unique pose resulted in low affinity observed by docking score value compared to our designed compounds and arylsulfamic acid ligand (Table 1, supplementary information).

The insulin resistance in type 2 diabetes is due to post receptor signal transduction defects. PTP1B has been reported to be a key negative regulator of insulin and leptin signaling pathways [31], Thus, the inhibition of PTP1B enhances the sensitivities of insulin and leptin and exhibited the protective effect on HFD induced obesity in the male western rat. The outcomes of biological evaluation either *in vitro* or *in vivo* are enough to confirm the activity of our synthesized compounds, which enhanced insulin sensitivity with declined plasma glucose and insulin levels. Moreover, the rats' body weight receiving HFD for two months were decreased with diminished cholesterol and TG levels.

3. Conclusion

Malfunctions in PTP1B activity are linked to various diseases including, cancer neurological disorders, diabetes, and obesity. Consequently, inhibition of this enzyme has emerged as a promising strategy for therapeutic intervention in the last two decades. The main obstacles limiting the application of PTP-1B inhibitors as an effective drug are poor cell permeability, declined bioavailability, and diminished selectivity. This study took in its consideration the multiple challenges and succeeded in overcoming them. Our rationale was to design double-binding inhibitor which, occupied catalytic and proximal sites to improve drug potency and selectivity. Benzene-sulfonamide derivatives had been designed and synthesized to occupy B-site with hydrophobic tail, Q-loop with urea or thiourea moiety, substrate recognition loop with an aromatic center, and catalytic site with new neutral scaffolds including, tetrazole, thiazolidinone, thiazinone, and chromenone. ESP, Mulliken charge distribution, and HOMO/LUMO analysis were useful tools in understanding the chemical reactivity of designed molecules with key residues of PTP1B. Treatment by the target compounds significantly improved the insulin resistance by restoring the insulin level, diminished plasma glucose level, decreasing body weight after HFD, and normalizing the serum lipid profile in a comparable manner with pioglitazone, a known PTP1B inhibitor. The designed compounds would be considered lead molecules which need further improvement to become promising drugs.

4. Material and methods

4.1. Instrument

Melting points were measured in open capillary tubes using Stuart melting point apparatus SMP10 (UK). Infrared (IR) spectra were recorded using KBr discs on a Shimadzu Spectrophotometer (λmax in $C\,m^{-1}$) (Kyoto, Japan). Proton Magnetic Resonance (^{1}HNMR) and Carbon Magnetic Resonance (^{13}CNMR) were recorded using the residual solvent signal as an internal standard with a Varian AS 400 (Varian Inc., Palo Alto, CA, USA). Chemical shifts are reported in d values (parts per million, ppm) relative to tetramethylsilane (TMS) as an internal standard. Abbreviations used in NMR analysis are as follows: d = doublet, m = multiplet, q = quartet, s = singlet, t = triplet. Electron impact mass spectra (EI-MS) were recorded on DI Analysis Shimadzu QP-2010 Plus mass spectrometer. Elemental analyses were recorded on Vario EL-CHNS Elemental Analyzer (GmbH, Germany). The results of elemental analyses (C, H, N) were found to be in good agreement (± 0.45%) with the calculated values. IR, EI-MS, and Elemental analyses were performed in the Microanalytical center, Cairo University, Egypt. While ^{1}HNMR and ^{13}CNMR were performed in the

graduate school of biomedical sciences, Nagasaki University, Japan. Reactions were monitored by thin layer chromatography (TLC) on Merck silica gel 60_{F254} and visualized with UV light. Ultrasonication was performed in ultrasound cleaner with a frequency of 50 kHz and an output power of 100 W.

4.2. Chemicals and reagents

Sulfadiazine, 4-amino-N-(pyrimidine-2-yl)benzenesulfonamide, phenyl isothiocyanate, phenyl isocyanate, chloroacetyl chloride, ethyl cyanoacetate, and acetylacetone were obtained from E. Merck (Germany) and S. D. Fine Chemicals (India). Ethyl isothiocyanate, ethyl-2-bromopropionate, phenacyl bromide, sodium azide, salicylaldehyde, sodium acetate, and ammonium acetate were purchased from Aldrich (USA). Solvents and other reagents were of pure grade and used without further purification.

4.3. Experimental

4.3.1. Chemistry

4.3.1.1. General procedure for synthesis of ureido and thioureido derivatives (1–3). A solution of 4-amino-N-(pyrimidin-2-yl) benzenesulfonamide (0.04 mol, 10 gm) in DMF (50 mL) was stirred and treated with the appropriate isothiocyanate or phenyl isocyanate (0.048 mol). the solution was refluxed for 24 h, DMF was removed under pressure, and the solid mass washed with water and purified by crystallization from ethanol.

4.3.1.2. 4-(3-phenylthioureido)-N-(pyrimidin-2-yl)benzenesulfonamide 1. M.p. = 195–197 °C, (yield 66%). IR (cm^{-1}): 1095(C═S), 1153(SO_2 *Sym*), 1327(SO_2 *Asym*), 1543(C═N), 1631(C═N), 3205(NH), 3356(NH), 3425(NH). Mass spectrum: *m/z*(%): 386(M^+ +1, 3.97%), 351(21.64%), 344(45.90%), 316(14.91%), 299(28.39%), 272(16.91%), 251(42.87%), 233(7.32%), 204(12.83%), 193(8.86%), 133(72.03%), 77(base peak, 100%). ^{1}H NMR (DMSO-d_6, 400 MHz): δ (ppm) 6.69 [d, 1H, H-pyrimidine], 7.11–7.6 (m, 9H, AR-H), 7.72–7.74 (d, 2H, H-pyrimidine), 8.59, 8.60[2 s, 2H, 2NH], 9.92 [s, 1H, SO_2NH].

4.3.1.3. 4-(3-phenylureido)-N-(pyrimidin-2-yl)benzenesulfonamide 2. M.p. = 298–300 °C, (yield 55%). IR (cm^{-1}): 1153(SO2 *Sym*), 1315(SO2 *Asym*), 1593(C═N), 1620(C═N), 1708(C═O), 3286(NH), 3329(NH), 3425(NH). Mass spectrum: *m/z*(%): 369(M^+, 1.05%), 346(4.93%), 313(4.71%), 292(1.20%), 253(10.21%), 211(30.91%), 185(base peak, 100%), 131(15.49%), 92(55.25%), 43(79.36%). ^{1}H NMR (DMSO-d_6, 400 MHz): δ (ppm) 6.70 [d, 1H, H-pyrimidine], 7.07–8 (m, 9H, AR-H), 8.52–8.53 (d, 2H, H-pyrimidine), 8.71, 8.86[2 s, 2H, 2NH], 9.2 [s, 1H, SO_2NH].

4.3.1.4. 4-(3-ethylthioureido)-N-(pyrimidin-2-yl)benzenesulfonamide 3. M.p. = 210–213 °C, (yield 70%). IR (cm^{-1}): 1087(C═S), 1157(SO2 *Sym*), 1315(SO2 *Asym*), 1589(C═N), 1624(C═N), 3109(NH), 3360(NH), 3444(NH). Mass spectrum: *m/z*(%): 337(M^+, 0.83%), 273(1.48%), 240(1.92%), 227(base peak, 100%), 185(23.06%), 134(38.13%), 90(29.82%), 67(26.91%). ^{1}H NMR (DMSO-d_6, 400 MHz): δ (ppm) 1.16–1.26 [t, 3H, CH3], 2.62–3 [q, 2H,CH2], 6.70 [d, 1H, H-pyrimidine], 7.99–7.12 (m, 4H, AR-H), 8.59–8.64 (d, 2H, H-pyrimidine), 802, 9.95[2 s, 2H, 2NH], 11.83 [s, 1H, SO_2NH].

4.3.1.5. General procedure for preparation of MSE-1 to MSE-9. A solution of the corresponding thioureido- N-(pyrimidine-2-yl) benzenesulfonamide derivatives (0.01 mol) in ethanol (HPLC) (50 mL) was refluxed with chloroacetyl chloride or ethyl-2-bromopropionate or phenacyl bromide (0.01 mol) and sodium acetate (0.02 mol) for 12 h. The reaction mixture was then filtered while hot concentrated and allowed to cool. The product obtained washed with water and recrystallized from ethanol.

4.3.1.6. (Z)-4-(5-oxo-3-phenylthiazolidin-2-ylideneamino)-N-(pyrimidin-2-yl)benzenesulfonamide MSE-1. M.p. = 162–164 °C, (yield 66%). IR (cm^{-1}): 694(C−S), 1153(SO_2 *Sym*), 1373(SO_2 *Asym*), 1539(C═N), 1581(C═N), 1635(C═N), 1720(C═O), 3379(NH). Mass spectrum: *m/z*(%): 427(M^+ +2, 4.07%), 425(M^+, 4.95%), 393(5.19%), 361(48.05%), 325(8.16%), 311(11.96%), 287(17.98%), 262(15.83%), 240(15.76%), 225(11.64%), 186(39.84%), 156(16.94%), 135(17.67%), 119(28.91%), 104(75.55%), 77(96.27%), 55(base peak, 100%). ^{1}H NMR (DMSO-d_6, 400 MHz): δ (ppm) 3.89 [s, 2H, CH2-thiazolidinone], 6.96 [d, 1H, H-pyrimidine], 7.10–7.82 (m, 9H, AR-H), 8.52–8.51 (d, 2H, H-pyrimidine), 10.86 [s, 1H, SO_2NH]. Anal.Calcd. for $C_{19}H_{15}N_5O_3S_2$: C, 53.63; H, 3.55; N, 16.46; S, 15.07. Found: C, 53.51; H, 3.86; N, 16.37; S, 15.25.

4.3.1.7. (Z)-4-(5-oxo-3-phenyloxazolidin-2-ylideneamino)-N-(pyrimidin-2-yl)benzenesulfonamide MSE-2. M.p. = 220–224 °C, (yield 68%). IR (cm^{-1}): 1153(SO2 *Sym*), 1234(C−O−C), 1315(SO2 *Asym*), 1496(C═N), 1543(C═N), 1593(C═N), 1708(C═O), 3356(NH). Mass spectrum: *m/z*(%): 409(M^+, 0.91%), 395(0.93%), 369(24.16%), 353(3.99%), 324(7.09%), 313(6.70%), 299(3.46%), 267(3.68%), 250(base peak, 100%), 227(5.86%), 206(45.71%), 149(11.50%), 123(7.98%), 108(76.67%), 71(38.23%). ^{1}H NMR (DMSO-d_6, 400 MHz): δ (ppm) 2.62 [s, 2H, CH2-oxazolidinone], 6.69 [d, 1H, H-pyrimidine], 7.06–7.74 (m, 9H, AR-H), 8.59–8.60 (d, 2H, H-pyrimidine), 8.82 [s, 1H, SO_2NH]. Anal.Calcd. for $C_{19}H_{15}N_5O_4S$: C, 55.74; H, 3.69; N, 17.11; S, 7.83. Found: C, 55.72; H, 3.97; N, 17.32; S, 7.84.

4.3.1.8. (Z)-4-(3-ethyl-5-oxothiazolidin-2-ylideneamino)-N-(pyrimidin-2-yl)benzenesulfonamide MSE-3. M.p. = 123–124 °C, (yield 66%). IR (cm^{-1}): 732(C−S), 1138(SO_2 *Sym*), 1319(SO_2 *Asym*), 1554(C═N), 1589(C═N), 1620(C═N), 1681(C═O), 3113(NH). Mass spectrum: *m/z*(%): 379(M+ +2, 1.08%), 377(M^+, 5.01%), 292(1.83%), 273(1.69%), 257(2.69%), 226(base peak, 100%), 185(39.79%), 170(7.47%), 134(19%), 92(14.20%), 65(13.27%). ^{1}H NMR (DMSO-d_6, 400 MHz): δ (ppm) 1.15–130 [t, 3H, CH_3], 3.32–3.35 [q, 2H, CH2], 3.89 [s, 2H, CH_2-thiazolidinone], 6.69 [d, 1H, H-pyrimidine], 7.12–7.24 (m, 4H, AR-H), 8.67–8.59 (d, 2H, H-pyrimidine), 8.80 [s, 1H, SO_2NH]. ^{13}C NMR:14.68 (2) 21.75, 39.49 (3), 61.34, 113.67, 116.52 122.45, 130.33, 136.41, 153.30, 157.58, 159.38, 173.34. Anal.Calcd. for $C_{15}H_{15}N_5O_3S_2$: C, 47.73; H, 4.01; N, 18.55; S, 16.99. Found: C, 47.42; H, 4.30; N, 18.52; S, 16.79.

4.3.1.9. (Z)-4-(4-oxo-3-phenyl-1,3-thiazinan-2-ylideneamino)-N-(pyrimidin-2-yl)benzenesulfonamide MSE-4. M.p. = 192–195 °C, (yield 40%). IR (cm^{-1}): 694(C−S), 1153(SO2 *Sym*), 1327(SO2 *Asym*), 1496(C═N), 1539(C═N), 1581(C═N), 1693(C═O), 3356(NH). Mass spectrum: *m/z*(%): 439(M+, 2.26%), 436(M+ −3, 10.81%), 410(5.74%), 392(17.63%), 365(11.89%), 320(5.26%), 297(7.42%), 286(16.33%), 258(27.04%), 211(36.34%), 192(13.04%), 153(12.75%), 119(36.17%), 91(base peak, 100%). ^{1}H NMR (DMSO-d_6, 400 MHz): δ (ppm) 1.42–1.45 [t, 2H, CH2-thiazinone], 3.39–3.49 [t, 2H, CH_2-thiazinone], 6.67 [d, 1H, H-pyrimidine], 7.02–7.72 (m, 9H, AR-H), 8.55–8.56 (d, 2H, H-pyrimidine). Anal. Calcd. for $C_{20}H_{17}N_5O_3S_2$: C, 54.65; H, 3.90; N, 15.93; S, 14.59. Found: C, 54.34; H, 3.91; N, 15.65; S, 14.52.

4.3.1.10. (Z)-4-(4-oxo-3-phenyl-1,3-oxazinan-2-ylideneamino)-N-(pyrimidin-2-yl)benzenesulfonamide MSE-5. M.p. = 202–205 °C, (yield 20%). IR (cm^{-1}): 694(C−S), 1153(SO_2 *Sym*), 1327(SO_2 *sym*), 1496(C═N), 1539(C═N), 1581(C═N), 1693(C═O), 3356(NH). ^{1}H NMR (DMSO-d_6, 400 MHz): δ (ppm) 1.25 [t, 3H, CH3-ethyl], 2.62[*t, 2H, CH_2-thiazinone*]3.53 [t, 2H, CH_2-thiazinone], 3.62 [q, 2H, CH_2-ethyl], 6.68 [d, 1H, H-pyrimidine], 7.04–7.98 (m, 4H, AR-H), 8.57 (d, 2H, H-pyrimidine), 10.01 [s, 1H, SO_2NH]. Anal. Calcd. for $C_{16}H_{17}N_5O_3S_2$: C, 49.09; H, 4.38; N, 17.98; S, 16.38. Found: C, 48.93; H, 4.16; N, 17.85; S, 16.52.

4.3.1.11. (Z)-4-(3-ethyl-4-oxo-1,3-thiazinan-2-ylideneamino)-N-(pyrimidin-2-yl)benzenesulfonamide MSE-6. M.p. = 285–288 °C, (yield 30%). IR (cm^{-1}): 1153(SO_2 *Sym*), 1327(SO_2 *Asym*), 1496(C═N), 1539(C═N), 1581(C═N), 1693(C═O), 3356(NH). ^{1}H NMR (DMSO-d_6, 400 MHz): δ (ppm) 1.62–1.64 [t, 2H, CH2-oxazinone], 3.52 [t, 2H, CH_2-oxazinone], 3.89 [s, 2H, CH_2-thiazolidinone], 6.69 [d, 1H, H-pyrimidine], 7.12–7.62 (m, 9H, AR-H), 8.67–8.69 (d, 2H, H-pyrimidine), 8.80 [s, 1H, SO_2NH]. Anal. Calcd. for $C_{20}H_{17}N_5O_4S$: C, 56.73; H, 4.05; N, 16.54; S, 7.57. Found: C, 56.43; H, 3.98; N, 16.05; S, 7.72.

4.3.1.12. (Z)-4-(3,4-diphenylthiazol-2(3H)-ylideneamino)-N-(pyrimidin-2-yl) benzenesulfonamide MSE-7. M.p. = 217–220 °C, (yield 70%). IR (cm^{-1}): 694(C–S), 1153(SO_2 *Sym*), 1327(SO_2 *Asym*), 1489(C═N), 1577(C═N), 1616(C═N), 3356(NH). Mass spectrum: *m/z*(%): 486(M^+ + 1, 2.91%), 485(M+, 7.73%), 421(25.29%), 393(11.92%), 364(6.45%), 328(6.29%), 312(61.51%), 285(2.34%), 239(8.21%), 211(14.57%), 185(87.78%), 131(33.91%), 92(56.76%), 77(base peak, 100%). ^{1}HNMR (DMSO-d_6, 400 MHz): δ (ppm) 6.14 [s, 1H, broad-SO_2NH], 6.57[S, 1H, CH-thiazolidine], 6.67 [d, 1H, H-pyrimidine], 7.02–7.74 (m, 14H, AR-H), 8.55–8.56 (d, 2H, H-pyrimidine). Anal.Calcd. for $C_{25}H_{19}N_5O_2S_2$: C, 61.84; H, 3.94; N, 14.42; S, 13.21. Found: C, 61.81; H, 4.22; N, 14.70; S, 13.20.

4.3.1.13. (Z)-4-(3,4-diphenyloxazol-2(3H)-ylideneamino)-N-(pyrimidin-2-yl)benzenesulfonamide MSE-8. M.p. = 210–213 °C, (yield 71%). IR (cm^{-1}): 1145(SO_2 *Sym*), 1234(C–O–C), 1315(SO_2 *Asym*), 1462(C═N), 1516(C═N), 1523(C═N), 3329(NH). Mass spectrum: *m/z*(%): 469(M^+, 1.35%), 457(1.88%), 424(2.71%), 405(3.27%), 382(1.08%), 367(1.86%), 337(1.62%), 325(1.72%), 294(2.19%), 270(5.82%), 229(5.83%), 204(23.52%), 158(6.97%), 131(6.25%), 105(82.26%), 77(85.41%), 43(base peak, 100%). ^{1}HNMR (DMSO-d_6, 400 MHz): δ (ppm) 6.62[S, 1H, CH-thiazolidine], 6.69[d, 1H, H-pyrimidine], 7.12–7.77 (m, 14H, AR-H), 8.60–8.62 (d, 2H, H-pyrimidine). ^{13}CNMR 113.51, 11364, 116.77, 119.84, 120.03, 123.57, 128.75, 12945, 130.15, 130.90, 134.59, 135.57, 153.92, 154.12, 158.01, 159.4. Anal.Calcd. for $C_{25}H_{19}N_5O_3S$: C, 63.95; H, 4.08; N, 14.92; S, 6.83. Found: C, 63.64; H, 4.16; N, 14.73; S, 6.92.

4.3.1.14. (Z)-4-(3-ethyl-4-phenylthiazol-2(3H)-ylideneamino)-N-(pyrimidin-2-yl)benzenesulfonamide MSE-9. M.p. = 235–238 °C, (yield 75%). IR (cm^{-1}): 702(C–S), 1153(SO_2 *Sym*), 1327(SO_2 *Asym*), 1492(C═N), 1539(C═N), 1573(C═N), 3367(NH). Mass spectrum: *m/z*(%): 438(M^+ + 1, 12.69%), 437(M^+, 35.41%), 373(base peak, 100%), 345(30.03%), 295(11.66%), 279(11.57%), 251(7.57%), 223(7.09%), 198(81.07%), 176(26.27%), 134(33.72%), 104(18.41%). ^{1}HNMR (DMSO-d_6, 400 MHz): δ (ppm) 1.24 [t, 3H, CH_3-ethyl], 3.57[q, 2H, CH_2-ethyl], 5.59 [s, 1H, CH-thiazolidine], 6.69[d, 1H, H-pyrimidine], 7.04–8.22 (m, 9H, AR-H), 8.60–8.62 (d, 2H, H-pyrimidine). Anal.Calcd. for $C_{21}H_{19}N_5O_2S_2$: C, 57.65; H, 4.38; N, 16.01; S, 14.66. Found: C, 57.32; H, 4.42; N, 16.03; S, 14.34.

4.3.1.15. General procedure for the preparation of MSE-11. A mixture of 4-amino-N-(pyrimidin-2-yl)benzenesulfonamide (0.04 mol, 10 gm), ethyl cyanoacetate (0.048 mol, 5.4 mL) and DMF (50 mL) was refluxed for 20 hr. The solvent was evaporated under reduced pressure to complete dryness and crystallized from ethanol.

4.3.1.16. 2-cyano-N-(4-(N-pyrimidin-2-ylsulfamoyl)phenyl) acetamide. M.p. = 270–171 °C, (yield 74%). IR (cm^{-1}): 1153(SO_2 *Sym*), 1323(SO_2 *Asym*), 1492(C═N), 1581(C═N), 1651(C═O), 2276(C≡N), 3356(NH), 3421(NH). Mass spectrum: *m/z*(%): 317(M^+, 0.84%), 299(1.04%), 278(0.77%), 262(1.69%), 234(0.84%), 185(64.70%), 170(2.61%), 158(3.16%), 131(3.13%), 108(23.73%), 92(46.11%), 65(base peak, 100%). ^{1}HNMR (DMSO-d_6, 400 MHz): δ (ppm) 4.29 [s, 2H, CH_2-acetamide], 6.69[d, 1H, H-pyrimidine], 7.10–7.73 (m, 4H, AR-H), 8.52–8.53 (d, 2H, H-pyrimidine). Anal.Calcd. for $C_{13}H_{11}N_5O_3S$: C, 49.21; H, 3.49; N, 22.07; S, 10.10. Found: C, 49.02; H, 3.22; N, 21.83; S, 10.14.

4.3.1.17. General procedure for the preparation of MSE-12. Heating a mixture of 2-cyano-N-(4-(*N*-pyrimidine-2-yl-sulfamoyl)phenyl) acetamide (0.01 mol, 3.5 gm), sodium azide (0.03 mol, 2.15 gm) and ammonium chloride (0.03 mol, 1.75) in DMF (50 mL) for 30 h. The reaction mixture was cooled to room temperature and concentrated under reduced pressure. The solid residue was taken into water (25 mL) and stirred for half an hour. Solid obtained was filtered, washed with water and finally crystallized from ethanol.

4.3.1.18. N-(4-(N-pyrimidin-2-ylsulfamoyl)phenyl)-2-(1H-tetrazol-5-yl) acetamide. M.p. = 240–142 °C, (yield 40%). IR (cm^{-1}): 1157(SO_2 *Sym*), 1323(SO_2 *Asym*), 1408(C═N), 1442(C═N), 1489(C═N), 1581(C═N), 1651(C═O), 3259(NH), 3356(NH), 3425(NH). Mass spectrum: *m/z*(%): 360(M^+, 1.21%), 346(1.02%), 333(2.24%), 277(1.23%), 263(0.87%), 242(4.31%), 214(25.31%), 185(22.05%), 150(19.41%), 129(5.33%), 108(78.62%), 92(78.17%), 65(79.86%), 43(base peak, 100%). ^{1}HNMR (DMSO-d_6, 400 MHz): δ (ppm) 3.55 [s, 2H, CH_2-acetamide], 6.13[s, 1H, NH-acetamide], 6.69[d, 1H, H-pyrimidine], 7.73–7.75 (m, 4H, AR-H), 8.59 (d, 2H, H-pyrimidine). ^{13}CNMR 39.70, 112.39 (2), 112.59, 115.76, 125,10, 127.50, 130.6 (2), 153.26, 157.45, 158.45. Anal.Calcd. for $C_{13}H_{12}N_8O_3S$: C, 43.33; H, 3.36; N, 31.10; S, 8.90. Found: C, 43.62; H, 3.39; N, 31.41; S, 8.64.

4.3.1.19. General procedure for the preparation of MSE-13. A mixture of 2-cyano-N-(4-(*N*-pyrimidine-2-yl-sulfamoyl)phenyl)acetamide (0.0056 mol, 1.8 gm), acetylacetone (0.0068 mol, 0.68 mL), and piperidine (0.5 mL) was fused in an oil bath at 150 °C for 1 h, then refluxed with ethanol (HPLC) (50 mL) for 3 hr to give a product which was crystallized from ethanol. HPLC-UV was applied to evaluate the purity of MSE-13 (Supplementary information)

4.3.1.20. 4-(3-cyano-4,6-dimethyl-2-oxopyridin-1(2H)-yl)-N-(pyrimidin-2-yl)benzenesulfonamide. M.p. = 280–282 °C, (yield 30%). IR (cm^{-1}): 1157(SO_2 *Sym*), 1327(SO_2 *Asym*), 1543(C═N), 1581(C═N), 1651(C═O), 2198(C≡N), 3356(NH). Mass spectrum: *m/z*(%): 381(M^+, 1.64%), 364(7.91%), 341(1.93%), 325(6.42%), 312(18.64%), 289(6.81%), 259(20.54%), 248(14.64%), 233(7.85%), 210(5.11%), 185(31.94%), 143(16.41%), 131(85.46%), 104(41.55%), 77(58.54%), 44(base peak, 100%). ^{1}HNMR (DMSO-d_6, 400 MHz): δ (ppm) 1.44–1.53 [s, 3H, CH_3-pyridinone], 1.60–173[s, 3H, CH3– pyridinone], 5.49[s, 1H, H-pyridinone], 6.11–6.13 [d, 1H, H-pyrimidine], 6.74–7.40 (m, 4H, AR-H), 7.96–7.99 (d, 2H, H-pyrimidine). Anal.Calcd. for $C_{18}H_{15}N_5O_3S$: C, 56.68; H, 3.96; N, 18.36; S, 8.41. Found: C, 56.62; H, 4.02; N, 18.59; S, 8.61.

4.3.1.21. General procedure for the preparation of MSE-14. A mixture of equimolar amounts of 2-cyano-N-(4-(*N*-pyrimidine-2-yl-sulfamoyl) phenyl)acetamide (0.0056 mol, 1.8 gm), salicylaldehyde (0.0056 mol, 0.69 mL), and ammonium acetate (0.0085 mol, 0.65 gm) in ethanol (50 mL) was heated under reflux for 2 h. The solid product formed was collected by filtration and recrystallized from ethanol. HPLC-UV was applied to evaluate the purity of MSE-14 (Supplementary information)

4.3.1.22. 2-imino-N-(4-(N-pyrimidin-2-ylsulfamoyl)phenyl)–2H-chromene-3-carboxamide. M.p. > 300 °C, (yield 80%). IR (cm^{-1}): 1161(SO_2 *Sym*), 1276(C–O–C), 1334(SO_2 *Asym*), 1489(C═N), 1581(C═N), 1620(C═N), 1693(C═O), 3155(NH), 3452(NH), 3556(NH). Mass spectrum: *m/z*(%): 421(M^+, 0.76%), 368(2.31%), 354(7.25%), 339(1.54%), 313(3.25%), 289(58.50%), 262(8.11%), 234(1.13%), 185(93.21%), 171(68.14%), 141(8.75%), 108(29.52%), 92(52.30%), 65(base peak, 100%). ^{1}HNMR (DMSO-d_6, 400 MHz): δ (ppm) 5.18[s, 1H, H-iminochromene], 6.15–6.22 [d, 1H, H-

pyrimidine], 6.70–6.83 (m, 8H, AR-H), 7.20 (s, 1H, NH-imino), 7.63–7.67 (d, 2H, H-pyrimidine), 8.20[s, 1H, NH-SO_2NH]. ^{13}CNMR 112.52, 115.89, 117.03, 117.57, 119.65, 119.75, 122.03, 122.62,125.23, 129.48, 130.19, 132.95, 134.39, 136.48, 152.58, 153.38, 157.58, 158.76, 160.61, 161.07, 192.24. Anal.Calcd. for $C_{20}H_{15}N_5O_4S$: C, 57.00; H, 3.59; N, 16.62; S, 7.61. Found: C, 57.02; H, 3.41; N, 16.48; S, 7.59.

4.3.1.23. General procedure for the preparation of MSE-15. To a solution of 2-cyano-N-(4-(*N*-pyrimidine-2-yl-sulfamoyl)phenyl)acetamide (0.0056 mol, 1.8 gm) in acetic acid (30 mL) containing 0.5 g of fused sodium acetate, salicylaldehyde (0.0056 mol, 0.69 mL) was added. The mixture was heated under reflux for 4 h and the solid product obtained after cooling was collected by filtration and recrystallized from acetic acid.

4.3.1.24. 2-oxo-N-(4-(N-pyrimidin-2-ylsulfamoyl)phenyl)–2H-chromene-3-carboxamide. M.p. > 300 °C, (yield 60%). IR (cm^{-1}): 1157(SO_2 *Sym*), 1273(C—O—C), 1334(SO_2 *Asym*), 1489(C═N), 1581(C═N), 1666(C═O), 1693(C═O), 3240(NH), 3421(NH). Mass spectrum: *m/z* (%): 422(M^+, 2.52%), 404(5.02%), 388(9.31%), 354(25.60%), 342(4.27%), 323(5.68%), 290(base peak, 100%), 272(18.84%), 235(4.50%), 195(21.99%), 171(45.21%), 131(11.61%), 102(11.09%), 65(31.20%). ^{1}HNMR (DMSO-d_6, 400 MHz): δ (ppm) 5.18[s, 1H, NH-acetamide], 6.15–6.90 (m, 8H, AR-H), 7.25 (s, 1H, CH-chromenone), 7.63–7.67 (d, 2H, H-pyrimidine), 8.17[s, 1H, NH-SO_2NH]. ^{13}CNMR 112.48, 115.85, 116.15, 117.56, 119.63, 122.05, 122.60, 124.25, 125.22, 129.43, 130.15, 132.91, 134.35, 136.76, 138.22, 149.92, 152.36, 157.56, 160.50, 192.17. Anal.Calcd. for $C_{20}H_{14}N_4O_5S$: C, 56.87; H, 3.34; N, 13.26; S, 7.59. Found: C, 56.63; H, 3.64; N, 13.52; S, 7.67.

4.4. Biological evaluation

4.4.1. In vitro PTP1B inhibition

The PTP1B inhibitory activity of the most active compounds (**MSE-13** and **MSE-14**) was measured with CycLex®Protein Tyrosine Phosphatase PTP1B Fluorometric Assay Kit according to manufacturer procedure. Shortly, the mix of 40 μL of reaction buffer and 5 μL of target compounds or pioglitazone (different concentrations were performed by serial dilutions) was added to each well of 96-well microplate. Next 5 μL of human recombinant PTP1B enzyme solution (20 m units/ μL) was added and a reaction mixture was incubated for 15 min at RT. After incubation, 20 μL of development buffer and 5 μL of fluoro-phospho-substrate (20 μM) (X 10) were added. After 15 min of incubation at RT, 25 μL of stop solution was added to each well. The fluorescence was measured at 510–530 nm emission after excitation at 482–502 nm. Each experiment was performed in triplicate. The measurement of the inhibitory effect was calculated as:

$$\text{Inhibition\%} = \frac{\text{Fluorescence intensity of test compound}}{\text{Fluorescence intensity of solvent control}} \times 100$$

4.4.2. In vitro quantitative measurement of PTP1B in rat liver homogenate TEST PRINCIPAL

This kit was based on sandwich enzyme-linked immune-sorbent assay technology. The microtiter plate provided in this kit has been pre-coated with an antibody specific to PTP1B. Standards or samples (liver homogenate) are then added to the appropriate microtiter plate wells with a biotin-conjugated antibody specific to PTP1B. Next, Avidin conjugated to Horseradish Peroxidase (HRP) is added to each micro-plate well and incubated. After TMB substrate solution is added, only those wells that contain PTP1B, biotin-conjugated antibody and enzyme-conjugated Avidin will exhibit a change in color. The enzyme-substrate reaction is terminated by the addition of sulphuric acid solution and the color change is measured spectrophotometrically at a wavelength of 450 nm ± 10 nm. The concentration of PTP1B in the samples is then determined by comparing the O.D. of the samples to the standard curve. The complete assay procedure is available in the supplementary information.

4.4.3. Screening of Anti-obesity of Benzene-Sulfonamide derivatives

Male Wistar rats weighing 120–150 g were divided into eighteen groups, each containing five animals. Group (1) was fed normal pellet diet (12% of total calories as fats). This group was considered as a negative control group. Obesity was induced in all other six groups via receiving high-fat diet (HFD) for two months (58% of total calories as fat, 25% as protein, and 17% as carbohydrates).

Starting from day 11 after induction of obesity, all HFD groups returned to a normal diet and were treated differently for 4 weeks. Group (2), was considered as an obese control group. Group (3–18) received different test compounds and pioglitazone at dose 2 mg/kg body weight, p.o given by oral gavage. The synthesized compounds were dissolved in the suspension of 0.5% CMC. After 4 weeks of treatment and at the end of the experiment, rats have fasted overnight and the final body weight for each animal was recorded. Blood glucose was measured using samples by an Accu-chek glucometer (Roche Diagnostic, Germany). Rats were then anesthetized by injection of ketamine (80 mg/kg, i.p.), and blood samples were collected in dry tubes and allowed to stand for 30 min and then centrifuged for 5 min at 1000 × g to obtain the serum. Lipid profile; triglycerides and total cholesterol were determined by enzymatic colorimetric assay kits (Biodiagnostics, Egypt) using an ultraviolet-visible spectrophotometer (UV-1601-PC; Shimadzu, Japan). All the data are expressed as mean ± SEM. Data are analyzed by one-way ANOVA followed by Bonferroni's post hoc test and assumption was statistically verified using Q-Q plot (Fig. 6 supplementary information)

4.4.4. Determination of fasting serum insulin and calculation of HOMA-IR index

Fasting serum insulin was measured using enzyme-linked immunosorbent assay (ELISA) kit for insulin (Biorbyt, UK) following the manufacturer's protocol. The absorbance of the reaction product was read at 450 nm. Homeostasis Model Assessment-Insulin Resistance (HOMA-IR) was calculated by the equation: (Glucose × insulin)/405 [32], where fasting plasma glucose concentration is given in mg/dL and fasting plasma insulin level is given in μIU/mL.

4.5. Molecular modeling study

4.5.1. Protein preparation for docking study

In the present study, the X-ray crystal structure of the catalytic domain of PTP1B enzyme in complex with sulfamic acid inhibitor (PDB ID: 2F70) TCPTP (1L8K) were obtained from Protein Data Bank and further prepared by protein preparation wizards, which is accessible in Glide, Schrodinger 10.1. After ensuring chemical accuracy, the preparation component adds hydrogen and neutralizes side chains that are neither close to the binding cavity nor involve in the formation of salt bridges. The OPLS-2005 force field was used for this purpose and then the active site of the protein was defined. In the next step, water molecules were removed, and H atoms were added to the crystal structure, most likely positions of hydroxyl and thiol hydrogen atoms, protonation states and tautomers of the His residue and Chi 'flip' assignment for Asn, Gln, and His residues were selected by the protein assignment script provided by Schrodinger. Minimization was performed to relieve steric clashes using the OPLS2005 force field until the average root mean square deviation (RMSD) of the non-hydrogen atoms reached a maximum value of 0.3 Å [33–35].

4.5.2. Ligand preparation

All the compounds were constructed using the fragment library of Maestro 10.1 and prepared by using the LigPrep 2.1, which can produce

many structures from each input structure with various ionization states, tautomers, stereochemistries and ring conformations. The OPLS-2005 force field was used for optimization, which produces the low energy conformer of the ligand. Partial atomic charges were ascribed, and possible ionization states were released at a pH of 7.0. The OPLS_2005 force field was used for optimization for generation of low energy conformer of the ligand. The energy minimization was performed for each ligand until it reached RMSD cutoff of 0.01 Å. The resulting structures were then taken for performing modeling studies [36]

4.5.3. Molecular docking

To test the docking parameters all compounds were docked into the binding site of the catalytic domain of PTP1B enzyme in complex with sulfamic acid inhibitor (PDB ID: 2F70) and TCPTP (1L8K) using Grid-Based Ligand Docking with Energetics (Glide) software from Schrodinger 10.1. To soften the potential for non-polar parts of the receptor, we scaled van der Waal radii of receptor atoms by 0.8 with a partial atomic charge of 0.15. A grid box with coordinates X = 10, Y = 10 and Z = 10 was generated at the centroid of the active site. The ligands were docked with the active site using the 'extra-precision' glide docking (Glide XP) which docks ligands flexibly. Glide generates conformations internally and passes these through a series of filters. The methodology of XP docking has been explained elsewhere. The final best-docked structure was chosen using a Glide score function. The lowest-energy docked complex was found in most of the similar docking conformations. Finally, the lowest-energy docked complex was selected for further study [33–35].

4.5.4. Lipinski's rule for drug likeliness and in silico ADME prediction

Lipinski's rule of five evaluates drug-likeness or determines whether a chemical compound with a certain biological and/or pharmacological activity has properties that would make it a likely orally active drug in humans. The rule describes important pharmacokinetics properties in the human body, including its absorption, distribution, metabolism, and excretion (ADME). The drug-like behavior of the proposed compounds through the analysis of the pharmacokinetic profile of the compounds were predicted by using QikProp module (v4.2, Schrodinger 2015-1). The compounds prepared by the LigPrep module (v3.1, Schrodinger 2015-1) in the previous step were utilized for the calculation of pharmacokinetic parameters by QikProp v4.2. The program QikProp v4.3, utilizes the method of Jorgensen19 to compute pharmacokinetic properties and descriptors. pharmaceutically relevant properties and physically significant descriptors of all the synthesized compounds such as molecular weight, log p, H-bond donors, and H-bond acceptors were analyzed [37].

4.6. Computational caculation

All calculations were performed using density functional theory (DFT) method and the Gaussian 09 program package. The standard basis set, 6-311 + + G(d,p) levels of the theory was used for the geometry optimizations [38].

Conflicts of interest

Authors declared that there are no conflicts of interest.

Appendix A. Supplementary material

Supplementary data to this article can be found online at https://doi.org/10.1016/j.bioorg.2019.01.052.

References

[1] http://www.who.int/dg/speeches/2016/obesity-diabetes-disaster/en/.

[2] https://www.idf.org/our-network/regions-members/middle-east-and-north-africa/welcome.html.

[3] M. Bodmer, C. Meier, S. Krähenbühl, S.S. Jick, C.R. Meier, Metformin, sulfonylureas, or other antidiabetes drugs and the risk of lactic acidosis or hypoglycemia: a nested case-control analysis, Diabetes Care 31 (2008) 2086–2091.

[4] A.P. Combs, Recent advances in the discovery of competitive protein tyrosine phosphatase 1B inhibitors for the treatment of diabetes, obesity, and cancer, J. Med. Chem. 53 (2010) 2333–2344.

[5] N.K. Tonks, Protein tyrosine phosphatases: from genes, to function, to disease, Nat. Rev. Mol. Cell Biol. 7 (2006) 833–846.

[6] T.O. Johnson, J. Ermolieff, M.R. Jirousek, Protein tyrosine phosphatase 1B inhibitors for diabetes, Nat. Rev. Drug. Discov. 1 (2002) 696–709.

[7] L.D. Klaman, O. Boss, O.D. Peroni, J.K. Kim, J.L.J.L. Martino, J.M. Zabolotny, N. Moghal, M. Lubkin, Y.B. Kim, A.H. Sharpe, A. Stricker-Krongrad, B.G. Shulman, Neel, B.B. Kahn, Increased energy expenditure, decreased adiposity, and tissue-specific insulin sensitivity in protein–tyrosine phosphatase 1B-deficient mice, Mol. Cell. Biol. 20 (2000) 5479–5489.

[8] Z. Jia, D. Barford, A.J. Flint, N.K. Tonks, Structural basis for phosphotyrosine peptide recognition by protein tyrosine phosphatase 1B, Science 268 (1995) 1754–1758.

[9] A.D.B. Pannifer, A.J. Flint, N.K. Tonks, D. Barford, Visualization of the cysteinyl-phosphate intermediate of a protein-tyrosine phosphatase by x-ray crystallography, J. Biol. Chem. 273 (1998) 10454–10462.

[10] M. Stuible, K.M. Doody, M.L. Tremblay, PTP1B and TC-PTP: regulators of transformation and tumorigenesis, Cancer Metastasis Rev. 27 (2008) 215–230.

[11] R. He, L. Zeng, Y. He, Z. Zhang, Recent advances in PTP1B inhibitor development for the treatment of type 2 diabetes and obesity, in: R.M. Jones (Ed.), New Therapeutic Strategies for Type 2 Diabetes: Small Molecule Approaches, RSC Publisher, London, 2013.

[12] L. Bialy, H. Waldmann, Inhibitors of protein tyrosine phosphatases: next-generation drugs? Angew. Chem., Int. Ed. 44 (2005) 3814–3839.

[13] S. Lee, Q. Wang, Recent development of small molecular specific inhibitor of protein tyrosine phosphatase 1B, Med. Res. Rev. 27 (2007) 553–573.

[14] S. Zhang, Z.Y. Zhang, PTP1B as a drug target: recent developments in PTP1B inhibitor discovery, Drug Discov. Today 12 (2007) 373–381.

[15] S.R. Klopfenstein, A.G. Evdokimov, A.-O. Colson, N.T. Fairweather, J.J. Neuman, M.B. Maier, J.L. Gray, G.S. Gerwe, G.E. Stake, B.W. Howard, J.A. Farmer, M.E. Pokross, T.R. Downs, B. Kasibhatla, K.G. Peters, 1,2,3,4-Tetrahydroisoquinolinyl sulfamic acids as phosphatase PTP1B inhibitors, Bioorg. Med. Chem. Lett. 16 (2006) 1574–1578.

[16] K.K.D. Amarasinghe, A.G. Evidokimov, K. Xu, C.M. Clark, M.B. Maier, A. Srivastava, A. Colson, G.S. Gerwe, G.E. Stake, B.W. Howard, M.E. Pokross, J.L. Gray, K.G. Peters, Design and synthesis of potent non-peptidic inhibitors of HPTPbeta, Bioorg. Med. Chem. Lett. 16 (2006) 4252–4256.

[17] X. Li, L. Wang, D. Shi, The design strategy of selective PTP1B inhibitors over TCPTP, Bioorg. Med. Chem. 24 (2016) 3343–3352.

[18] E.R.H. Jones, F.A. Robinson, H.N. Starchan, Some 5-spirothiazolidiones, J. Chem. Soc. (1946) 91–92.

[19] A.R. Gholap, K.S. Toti, F. Shirazi, R. Kumari, M.K. Bhat, M.V. Deshpande, K.V. Srinivasan, Synthesis and evaluation of antifungal properties of a series of the novel 2-amino-5-oxo-4-phenyl-5,6,7,8-tetrahydroquinoline-3-carbonitrile and its analogues, Bioorg. Med. Chem. 15 (2007) 6705–6715.

[20] Kh.A.M. El-Bayouki, M.M. Aly, Y.A. Mohamed, W.M. Basyouni, S.Y. Abbas, Novel 4 (3H)-quinazolinones containing biologically active thiazole, pyridinone and chromene of expected antitumor and antifungal activities, Eur. J. Chem. 2 (2011) 455–462.

[21] A. Sharon, R. Pratap, P. Tiwari, A. Srivastava, P.R. Maulik, V. Ram, Synthesis and in vivo antihyperglycemic activity of 5-(1H-pyrazol-3-yl)methyl-1H-tetrazoles, Bioorg. Med. Chem. Lett. 15 (2005) 2115–2117.

[22] P. Heneberg, Use of protein tyrosine phosphatase inhibitors as promising targeted therapeutic drugs, Curr. Med. Chem. 16 (2009) 706–733.

[23] Y.A. Puius, Y. Zhao, M. Sullivan, D.S. Lawrence, S.C. Almo, Z.Y. Zhang, Identification of a second aryl phosphate-binding site inProtein-tyrosine phosphatase 1B: a paradigm for inhibitor design, PNAS 94 (1997) 13420–13425.

[24] P. Huang, J. Ramphal, J. Wei, C. Liang, B. Jallal, G. McMahon, C. Tang, Structure-based design and discovery of novel inhibitors of protein tyrosine phosphatases, Bioorg. Med. Chem. 11 (2003) 1835–1849.

[25] N. Lakshminarayana, Y.R. Prasad, L. Gharat, A. Thomas, S. Narayanan, A. Raghuram, C.V. Srinivasan, B. Gopalan, Synthesis and evaluation of some novel dibenzo[b, d]furan carboxylic acids as potential anti-diabetic agents, Eur. J. Med. Chem. 45 (2010) 3709–3714.

[26] Z. Xin, G. Liu, C. Abad-Zapatero, Z. Pei, B. Szczepankiewicz, X. Li, T. Zhang, C.W. Hutchins, P.J. Hajduk, S.J. Ballaron, M.A. Stashko, T.H. Lubben, J.M. Trevillyan, M.R. Jirousek, Identification of a monoacid-Based, cell permeable, selective inhibitor of protein tyrosine phosphatase 1B, Bioorg. Med. Chem. Lett. 13 (2003) 3947–3950.

[27] J. Liu, F. Jiang, Y. Jin, Y. Zhang, J. Liu, W. Liu, L. Fu, Design, synthesis, and evaluation of 2-substituted ethenesulfonic acid ester derivatives as protein tyrosine phosphatase 1B inhibitors, Eur. J. Med. Chem. 57 (2010) 10–20.

[28] A.K. Saxena, G. Pandey, S. Gupta, A.B. Singh, A.K. Srivastava, Synthesis of protein tyrosine phosphatase 1B inhibitors: model validation and docking studies, Bioorg. Med. Chem. Lett. 19 (2009) 2320–2323.

[29] M.S. Malamas, J. Sredy, I. Gunawan, B. Mihan, D.R. Sawicki, L. Seestaller, D. Sullivan, B.R. Flam, New azolidinediones as inhibitors of protein tyrosine phosphatase 1B with antihyperglycemic properties, J. Med. Chem. 43 (2000) 995–1010.

[30] Z. Wang, Z. Liu, W. Lee, S.N. Kim, G. Yoon, S.H. Cheon, Design, synthesis and docking study of 5-(substituted benzylidene)thiazolidine-2,4-dione derivatives as inhibitors of protein tyrosine phosphatase 1B, Bioorg. Med. Chem. Lett. 24 (2014) 3337–3340.
[31] M. Elchebly, P. Payette, E. Michaliszyn, W. Cromlish, S. Collins, A.L. Loy, D. Normandin, A. Cheng, J. Himms-Hagen, C.C. Chan, C. Ramachandran, M.J. Gresser, M.L. Tremblay, B.P. Kennedy, Increased insulin sensitivity and obesity resistance in mice lacking the protein tyrosine phosphatase-1B gene, Science 283 (1999) 1544–1548.
[32] D.R. Matthews, J.P. Hooker, A.S. Rudenski, Homeostasis model assessment: insulin resistance and B-cell function from fasting plasma glucose and insulin concentration in man, Diabetologia 28 (1985) 412–419.
[33] T.A. Halgren, R.B. Murphy, R.A. Friesner, et al., Glide: a new approach for rapid, accurate docking and scoring. 2. Enrichment factors in database screening, J. Med. Chem. 47 (2004) 1750–1759.
[34] R.A. Friesner, J.L. Banks, R.B. Murphy, et al., Glide: a new approach for rapid, accurate docking and scoring. 1. Method and assessment of docking accuracy, J. Med. Chem. 47 (2004) 1739–1749.
[35] R. Abdelhameed, M.S. Elgawish, A. Mira, et al., Anti-choline esterase activity of ceramides from the Red Sea marine sponge Mycale euplectellioides, RSC Adv. 6 (2016) 20422–20430.
[36] https://isp.ncifcrf.gov/files/isp/uploads/2010/07/lp23_user_manual.pdf.
[37] https://www.schrodinger.com/qikprop.
[38] M.J. Frisch, G.W. Trucks, H.B. Schlegel, et al., Gaussian 09W, Revision C.01, Gaussian, Inc., Wallingford CT, 2013.